A multiple timescale approach of bispectral correlation

V. Denoël[a], M. Esposito Marzino[a], M. Geuzaine[a,b,*]

[a] *Structural & Stochastic Dynamics, Structural Engineering Division, University of Liège, Liège, Belgium*
[b] *F.R.S.-FNRS, National Fund for Scientific Research, Brussels, Belgium*

Abstract

The paper develops an approximate semi-analytical solution for the computation of the third statistical cross-moments of modal responses in a stochastic dynamic analysis. These moments would require heavy twofold numerical integration in a general context but are drastically simplified in the proposed formulation by taking advantage of the assumed distinctness between the low characteristic frequency of the loading and the natural frequencies of the structure. This condition is typically respected and acknowledged in wind engineering where the buffeting analysis of large structure hinges on the Background/Resonant decomposition. As such, the proposed formulation extends to third statistical order the existing developments for the estimation of the modal variances and covariances. It allows the third order spectral analysis of large structures to be conducted within a reasonable amount of time. It also reveals the existence of three main components to the response: background, bi-resonant and tri-resonant. The latter one is specific to this very own problem and is shown to be important when the sum of two natural frequencies is equal to a third one, although the structural behavior is linear. Mathematics highlight this and other findings which are then illustrated on a minimum working example, easily reproducible by readers. Overall, it clearly demonstrates the benefits of the proposed decomposition in terms of both behavioural comprehension and computational consumption.

Keywords: background, resonant, non Gaussian, MTSA Multiple Timescale Spectral Analysis, Complete Cubic Combination, Cubic Root of the Sum of the Cubes

1. Introduction

Spectral analysis is a well-known type of structural analysis that consists in computing the steady-state variance of the response of a (usually linear) system subject to stationary random excitations [1, 2, 3]. In such an analysis, the variances of the problem responses are obtained as the integrals of the corresponding power spectral densities (PSDs), which are themselves obtained as the product of PSDs of loading and frequency response functions. In the standard formulation, the analysis concerns steady-state responses and is therefore widely deployed by the wind engineering community which typically considers the buffeting wind loads to be Gaussian and stationary [4, 5]. Other applications of the spectral analysis concern the vibrations of pipes under turbulent internal or external flows [6], or vibrations due to random excitations of machinery [7], or even vibrations resulting from some types of human loading [8].

The dynamic structural analysis is usually performed in a modal basis, which is known to provide optimal convergence rate for a loading covering the resonance frequencies [9]. The spectral analysis is therefore ad-

*corresponding author, preprint submitted to Journal of Wind Engineering and Industrial Aerodynamics, December 26, 2022
Email address: v.denoel@uliege.be; michele.espositomarzino@uliege.be; mgeuzaine@uliege.be (M. Geuzaine)

vantageously led in the basis of normal modes. This allows model reduction since the deformed configuration of the structure is sought in a subspace of the space of nodal coordinates. This yields a drastic reduction of the number of kinematic unknowns in the problem, typically from a few hundreds of thousands of nodal degrees-of-freedom, to dozens of modal coordinates. The responses in the different modes are usually not uncorrelated, either because there exists some coherence in the modal loads and natural frequencies are close to each other [10], either because damping is non classical [11]. Hence correlation is not systematically negligible. Fortunately, it is possible to estimate the correlation coefficients [12] and to use them while recombining the modal responses. In seismic engineering, the most complete recombination is termed the Complete Quadratic Combination (CQC) [13]. It degenerates into the Square Root of the Sum of the Square (SRSS) recombination when modal correlations are neglected.

A typical spectral analysis is limited to second statistical order, i.e. PSDs. Higher order versions of this spectral analysis do exist [14]. They are based on the concept of bispectrum and trispectrum; in this paper we will restrict ourselves to the third statistical order, i.e. bispectra. This spectral analysis of higher order has been widely applied in the signal analysis of waves [15] and in change detections in condition monitoring [16]. In this paper, we focus on the bispectral analysis, which consists in analyzing how the third statistical moment of the input in a dynamical system is filtered by the system. In structural engineering, this type of analysis is useful when the loads applied on structures are non Gaussian (hence represented by their successive statistical moments, of order higher than 2), as it is also the case in wind engineering [17, 18, 19, 20, 21] or marine engineering [22, 23]. Similarly to the spectral analysis which requires integration of the PSD to obtain a variance, in the bispectral analysis, the third statistical moment of any quantity is obtained by the integral of the corresponding bispectrum. In particular, unilateral bispectra of modal coordinates will provide the third statistical moment of the modal responses and eventually their skewness coefficient [24, 25]. A slightly more advanced concept is that of cross-bispectrum which indicates the distribution of a cross-moment (e.g. between modal responses) in the frequency space. A high order spectral analysis toolbox has been implemented in Matlab [26] 25 years ago, which has helped disseminating the concepts and dragging the interests of researchers in using bispectral analysis.

At this stage, it should be understood that the statistical moments of the response are obtained as integrals of spectral quantities: unilateral and cross-PSDs at second order and unilateral and cross-bispectra at third order. The computation burden associated with the numerical estimation of these integrals is typically massive. In order to simplify the computation of these integrals it is possible to take advantage of the existence of multiple timescales in the problem. This has for instance resulted in the famous Background/Resonant decomposition in Wind Engineering applications [27], which is fundamentally similar to the short correlation approximation in time domain approaches based on the Fokker-Planck-Kolmogorov equation [28]. At the time where this decomposition was developed, for the computation of the variance of single oscillators, this smart approach was the only possible solution to numerically integrate the unilateral PSDs of modal responses in a reasonable and competitive amount of time. Of course, with the known increase of computational power, these integrals are now computed in a glimpse. Yet, the very same problem is now shifted to the estimation of the third statistical

response, which is still computationally demanding today, due to the curse of dimensionality. Moreover, while the third order (bispectral) analysis of large systems seems to be conceivable today, the fourth order analysis remains out of reach for now [29, 30].

The Background/Resonant decomposition and the short correlation time approximation have inspired the development of a more general approach, the Multiple Timescale Spectral Analysis (MTSA) [31], which offers similar computational speedup for a bunch of applications in a broader context. Fortunately, this more general theory is also applicable to the third order (bispectral) analysis of large structures. It shall therefore alleviate the high computational power associated with bispectral analysis and eventually turn hours of computation into minutes. Former developments have already indicated the possibility to apply the MTSA to the third statistical order of the response of a single oscillator [24, 25], and have highlighted the existence of a background and a bi-resonant component in the response. This concept can be directly translated to modal responses and, in order to be able to recombine them in an accurate manner, considering the necessary correlation between modal responses, the only missing piece was the modal correlation at third order. This quantity, also named *bicorrelation*, extends to third statistical order the well-known concept of covariance and correlation.

This paper precisely focuses on the multiple timescales approximation of the bicorrelation. It is focused on applications where the characteristic frequency of the loading is much lower than the natural frequencies of the structure, which is typical in buffeting analysis. As shown below, it results in a simple expression for the cross-correlations of modal responses at third order, which makes it possible to recombine modal responses in the sense of a Complete Cubic Combination. The paper is organized as follows. Section 3 gives the mathematical statement of the considered problem. In Section 4, the main specificities of the problem are summarized, especially with regards to symmetry properties and existence of small numbers. The Multiple Timescale Spectral Analysis is then developed in Section 5 for the computation of cross-correlations at third order. Two academic examples of application are given in Section 6 to contribute to the validation and illustration of the proposed method.

2. Nomenclature

Bold lowercase symbols designate vectors (e.g. $\mathbf{q}(t)$); bold uppercase symbols designate matrices (e.g. $\mathbf{M}^\star$). There is one exception to this rule: the $n_\mathrm{m} \times n_\mathrm{m}$ matrices of second order moments (covariance matrices) are written with lowercase symbols. For instance, the covariance matrix of modal responses is written $\mathbf{m}_{2,q}$. Its elements are noted $m_{2,q_{ij}}$ in the most general case. Diagonal elements are written $m_{2,q_{ii}}$ or, equivalently m_{2,q_i} (without repeating the index). Similarly, the $n_\mathrm{m} \times n_\mathrm{m} \times n_\mathrm{m}$ tensor of third order moments is written $\mathbf{m}_{3,q}$. Any canonical element is noted $m_{3,q_{ijk}}$, and m_{3,q_i} specifically refers to super-diagonal elements ($i = j = k$). Indices i, j, k and m are used to denote modes while index n represents a (nodal) degree-of-freedom. The complex imaginary unit is noted i.

3. Mathematical Statement

3.1. Governing equations

The dynamics of a structural system in its modal basis is modeled by the equation of motion

$$\mathbf{M}^\star \ddot{\mathbf{q}}(t) + \mathbf{C}^\star \dot{\mathbf{q}}(t) + \mathbf{K}^\star \mathbf{q}(t) = \mathbf{p}(t) \tag{1}$$

where $\mathbf{M}^\star$, $\mathbf{C}^\star$ and $\mathbf{K}^\star$ are structural modal matrices (mass, viscosity and stiffness, respectively). Matrices $\mathbf{M}^\star$ and $\mathbf{K}^\star$ are diagonal as soon as the normal modes of vibration are used [9]. These modes are gathered in an $n_{\text{dof}} \times n_{\text{m}}$ matrix $\mathbf{\Phi}$ where n_{dof} and n_{m} respectively represent the number of degrees-of-freedom in the structural model and the number of modes used for the analysis ($n_{\text{m}} \ll n_{\text{dof}}$ for typical large scale structures). In practice, the modal damping matrix $\mathbf{C}^\star$ could be fully populated but has small off-diagonal elements in most cases of application [9]. These terms could be neglected or treated in a fashion similar to that presented in [10, 32] and transform the problem into an equivalent one with a diagonal damping matrix and an equivalent loading. In the current context, it is therefore assumed that all three modal structural matrices are diagonal so that the modal responses $q_m(t)$ are determined independently for each modal loading $p_m(t)$. In the frequency domain [9], Equation (1) reads

$$\mathbf{q}(\omega) = \mathbf{H}(\omega)\,\mathbf{p}(\omega) \tag{2}$$

where the frequency response function $\mathbf{H}(\omega) = \left(-\mathbf{M}^\star\omega^2 + \mathrm{i}\omega\mathbf{C}^\star + \mathbf{K}^\star\right)^{-1}$ is also a diagonal matrix and each of its diagonal elements, for $m = 1, \cdots, n_{\text{m}}$, is expressed as

$$H_m(\omega) = \frac{1}{k_m} \frac{1}{1 + 2\mathrm{i}\xi_m \frac{\omega}{\omega_m} - \left(\frac{\omega}{\omega_m}\right)^2} \tag{3}$$

where $k_m \equiv K_m^\star$, ξ_m and ω_m are the modal stiffness, the damping ratio and the circular natural frequency in mode m.

Once the modal responses are obtained, they can be recombined in order to determine the quantities of interest for the design: displacements, internal forces, reactions at supports. For instance, the displacement or rotation at degree-of-freedom n is expressed by

$$x_n(t) = \sum_{m=1}^{n_{\text{m}}} \phi_{nm} q_m(t)\,. \tag{4}$$

where ϕ_{nm} is the magnitude of degree-of-freedom n in mode m . This equation offers a canonical form, applicable to other structural responses than displacements and rotations. Indeed, in a linear structural analysis any other response such as internal forces and ground reactions is obtained with a similar linear combination. By giving ϕ_{nm} the meaning of any other modal response, Equation (4) is therefore applicable to any structural response in a wide sense. The same relation holds in the frequency domain as a consequence of the linearity of the operators.

3.2. Second order stochastic analysis

In a stochastic context, the modal loading $\mathbf{p}(t)$ is represented as a stochastic process. It is assumed that this process is zero-mean, stationary in time but possibly non Gaussian so that it is fully described by its spectra of various orders [14, 24, 25]. This assumption is justified as follows: (i) the case of a non-zero-mean process can be tackled similarly owing to the linearity of the problem and the superposition principle, (ii) stationarity in time is a common assumption for wind loads [4], wave and current loads [33], (iii) the non Gaussianity of the loading might arise from the nonlinear nature of the wind and wave loading processes [34, 35].

The second-order spectrum $S(\omega)$ of a stochastic process is commonly called the *power spectral density* (PSD). The integral of this spectrum over the frequency domain provides the variance (second moment) of the process $m_2 \equiv \sigma^2$. For instance the variance of the modal loading in mode i (m_{2,p_i}) and the variance of the modal response in mode i (m_{2,q_i}) are obtained by

$$m_{2,p_i} = \int_{-\infty}^{+\infty} S_{p_i}(\omega)\,\mathrm{d}\omega \quad ; \quad m_{2,q_i} = \int_{-\infty}^{+\infty} S_{q_i}(\omega)\,\mathrm{d}\omega \tag{5}$$

where $S_{p_i}(\omega)$ and $S_{q_i}(\omega)$ are the corresponding power spectral densities, which are related by

$$S_{q_i}(\omega) = |H_i(\omega)|^2 S_{p_i}(\omega). \tag{6}$$

Modal loads are not necessarily uncorrelated. Their correlation (as well as those of any two processes) is expressed by means of the covariance which is obtained by integration of a cross-power spectral density [1, 14]. For instance the covariance of the modal loads in modes i and j and the covariance of the modal responses in modes i and j are expressed as

$$m_{2,p_{ij}} = \int_{-\infty}^{+\infty} S_{p_{ij}}(\omega)\,\mathrm{d}\omega \quad \text{and} \quad m_{2,q_{ij}} = \int_{-\infty}^{+\infty} S_{q_{ij}}(\omega)\,\mathrm{d}\omega \tag{7}$$

respectively, or in terms of each modal variance and a correlation coefficient as $m_{2,ij} = \rho_{ij}\sqrt{m_{2,i}m_{2,j}}$. The subtle difference between (5) and (7) thus lies in the use of one or two indices to refer to variances or covariances. Anyway, when $i = j$, (7) degenerates into (5), i.e. $m_{2,p_{ii}} \equiv m_{2,p_i}$ and similarly for the modal responses. In (7), $S_{p_{ij}}(\omega)$ and $S_{q_{ij}}(\omega)$ represent the cross-power spectral densities of the modal loads and modal responses, which are related by

$$S_{q_{ij}}(\omega) = H_i(\omega)\,\overline{H}_j(\omega)\,S_{p_{ij}}(\omega) \tag{8}$$

where the overline is used for the conjugate operator [1]. Equations (6) and (8) are the stochastic equivalent of (2) at second statistical order; they express the modal responses (and their correlations) to a given loading.

The stochastic version of the recombination operation (4) is managed by considering the structural response x_n and the modal responses q_m as random variables. Using the symbol $\mathbb{E}[\cdot]$ to represent the expectation operator, the second moment of the structural response reads

$$m_{2,x_n} = \mathbb{E}\left[x_n^2\right] = \mathbb{E}\left[\sum_{i=1}^{n_\mathrm{m}} \phi_{ni} q_i \sum_{j=1}^{n_\mathrm{m}} \phi_{nj} q_j\right] = \sum_{i=1}^{n_\mathrm{m}}\sum_{j=1}^{n_\mathrm{m}} \phi_{ni}\phi_{nj}\mathbb{E}[q_i q_j] = \sum_{i=1}^{n_\mathrm{m}}\sum_{j=1}^{n_\mathrm{m}} \phi_{ni}\phi_{nj} m_{2,q_{ij}}. \tag{9}$$

Notice that the mean square response is equal to the variance since the average response is equal to zero, $\mathbb{E}[x_n] = 0$ and $\mathbb{E}[q_i] = 0$, $\forall i = 1, \cdots, n_{\mathrm{m}}$. It is has been shown in [24] that the covariance of modal responses $m_{2,q_{mn}}$ is small (compared to the corresponding variances) when the modal loads are not correlated (in case of background response) or when the natural frequencies are relatively more distant than the damping ratio or the modal forces are not coherent in the neighborhood of the natural frequencies of the two considered modes (in case of resonant response). This motivates to write the variance of structural responses as

$$m_{2,x_n} = \sum_{i=1}^{n_{\mathrm{m}}} \phi_{ni}^2 m_{2,q_i} + \sum_{i=1}^{n_{\mathrm{m}}} \sum_{j=1, i\neq j}^{n_{\mathrm{m}}} \phi_{ni}\phi_{nj} m_{2,q_{ij}} \tag{10}$$

where the contribution of the variances (m_{2,q_i}) and covariances ($m_{2,q_{ij}}$, $i \neq j$) of modal responses are explicitly highlighted, in the two terms respectively. In seismic engineering [36], truncation after the first (single) summation is usually called the Square Root of the Sum of Squares (SRSS) combination, while the full expression is called the Complete Quadratic Combination (CQC). The latter one is attributed to the works of der Kiureghian [37].

It is of utmost importance to quantify the covariance of modal responses $m_{2,q_{ij}}$ in the critical configurations where the second term in (10) is not negligible. A full integration of the corresponding spectra, as in (7), is of course an option but an optimized approach based on the background and resonant decomposition is naturally faster, whenever applicable. This decomposition is well-known in the wind engineering community, especially for the single degree-of-freedom case, where after the works of Liepmann [38] and wide-spreading of Davenport [27], the variance of a modal response m_{2,q_i} is expressed as

$$m_{2,q_i} \simeq \frac{m_{2,p_i}}{k_i^2} + \frac{S_{p_i}(\omega_i)}{k_i^2}\frac{\pi\omega_i}{2\xi_i}, \tag{11}$$

where, in the background component, $m_{2,p_i} = \sigma_{p_i}^2$ and, in the resonant component, $S_{p_i}(\omega_i)$ represents the unilateral PSD of the modal load evaluated at the i^{th} natural frequency. Although less well known, the same decomposition exists for the covariance of modal responses [12]

$$m_{2,q_{ij}} \simeq \frac{m_{2,p_{ij}}}{k_i k_j} + \frac{1}{k_i k_j}\frac{S_{p_{ij}}(\omega_i) + S_{p_{ij}}(\omega_j)}{2}\psi(\omega_i, \omega_j, \xi_i, \xi_j) \tag{12}$$

where $\psi(\omega_i, \omega_j, \xi_i, \xi_j)$ is a coefficient that translates the relative proximity of natural frequencies; when $i = j$, $\psi = \frac{\pi\omega_i}{2\xi_i}$; furthermore $\psi \to 0$ as ω_i and ω_j tend away from each other. In any case, (12) generalizes (11).

The decomposition (12) is valid under the condition that the structure is lightly damped (say less than 10% of critical damping) and the characteristic frequencies of the loading and the natural frequencies are well separated. This equation shows that the full integration can be avoided and the covariances of modal responses can in fact be estimated at a marginal cost, which therefore justifies the systematic use of the complete quadratic combination, i.e. both terms in (10).

3.3. Third order stochastic analysis

The third-order spectrum $B(\omega_1, \omega_2)$ of a stochastic process is commonly called the *bispectrum*. More generally, we may introduce the cross-bispectrum right away, which represents the distribution of the third cross-moment in the frequency space. Indeed, the twofold integral of this spectrum over the frequency domain

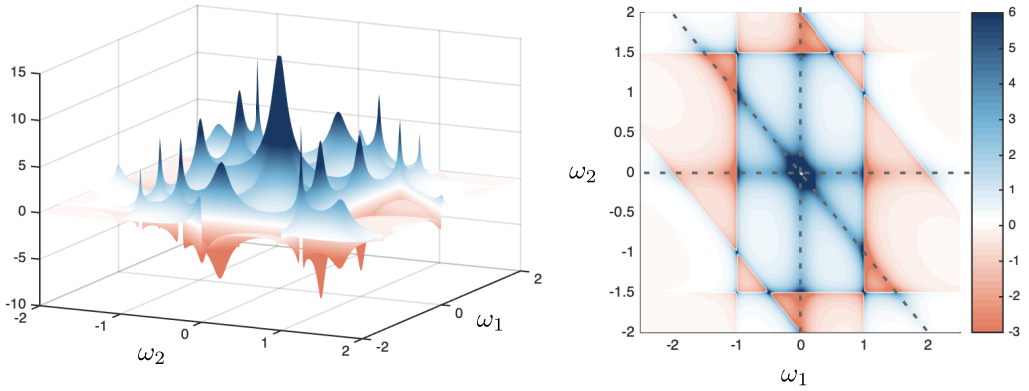

Figure 1: Illustrations of the multiple peaks in the cross-bispectrum of modal responses $B_{q_{ijk}}(\omega_1, \omega_2)$ — Numerical values, kernel: $\omega_i = 1$, $\omega_j = 1.5$, $\omega_k = 2$, $\xi_i = \xi_j = \xi_k = 0.02$, loading (same as first illustration in Section 6): $\alpha = 0.1$, all other parameters equal to 1. Dashed lines in the right pane indicate the ridges of the bispectrum of the loading.

provides the third cross-moment of the processes. For instance, the cross-moments of the modal loads and modal responses are given by

$$m_{3,p_{ijk}} = \iint_{\mathbb{R}^2} B_{p_{ijk}}(\omega_1, \omega_2)\, \mathrm{d}\omega_1 \mathrm{d}\omega_2 \quad ; \quad m_{3,q_{ijk}} = \iint_{\mathbb{R}^2} B_{q_{ijk}}(\omega_1, \omega_2)\, \mathrm{d}\omega_1 \mathrm{d}\omega_2 \tag{13}$$

where $B_{p_{ijk}}(\omega_1, \omega_2)$ and $B_{q_{ijk}}(\omega_1, \omega_2)$ are the cross-bispectra of the modal loads and modal responses. They are related to each other by

$$B_{q_{ijk}}(\omega_1, \omega_2) = \mathcal{K}_{ijk}(\omega_1, \omega_2)\, B_{p_{ijk}}(\omega_1, \omega_2) \tag{14}$$

where the kernel $\mathcal{K}_{ijk}(\omega_1, \omega_2)$ is defined by

$$\mathcal{K}_{ijk}(\omega_1, \omega_2) = H_i(\omega_1)\, H_j(\omega_2)\, \overline{H}_k(\omega_1 + \omega_2)\,. \tag{15}$$

Similarly to (6) and (8), Equation (14) is the stochastic equivalent of (2), but at third statistical order. With shorter notations, the major difficulty in the stochastic analysis consists in computing the integral

$$m_{3,q_{ijk}} = \iint_{\mathbb{R}^2} \mathcal{K}_{ijk}(\omega_1, \omega_2)\, B_{p_{ijk}}(\omega_1, \omega_2)\, \mathrm{d}\omega_1 \mathrm{d}\omega_2. \tag{16}$$

Notice that the subscripts "3" and "q" will then be omitted to simplify notations; no confusion is possible since the rest of the paper exclusively focuses on third statistical moments of modal responses q and the evaluation of this integral. Super-diagonal elements of this 3-D matrix ($i = j = k$) contain the third statistical moments of the modal responses. All off-diagonal elements contain cross-moments which, again, are necessary to compute the statistics of linear combinations of modal responses.

The integral in (16) is not necessarily easy to compute because of the multiple, and possibly sharp, peaks in the kernel $\mathcal{K}_{ijk}$ and in the bispectrum of the loading $B_{p_{ijk}}$, see Figure 1. More details about all these peaks follow in Section 5.1.

The Multiple Timescale Spectral Analysis [31] is a very general and versatile technique that is able to cope with such integrals. It is used in this paper to transform this two-fold integral into a single one and

make the computation of the third statistical moment much faster, while offering at the same time a clear understanding of the origin of modal (bi-)correlation. As stated in the introduction, super-diagonal elements ($i = j = k$) correspond to the single degree-of-freedom case and have already been studied previously both with respect to the real part of the bispectrum [24] and more recently with respect to its imaginary part [39]. This approximation,

$$m_{3,q_i} = \frac{m_{3,p_i}}{k_i^3} + 6\pi \frac{\xi_i \omega_i^3}{k_i^3} \int_{\mathbb{R}} \frac{\mathrm{Re}\left[B_{p_i}\left(\omega_i, \omega_2\right)\right]}{\left(2\xi_i\omega_i\right)^2 + \omega_2^2} \,\mathrm{d}\omega_2 + 3\pi \frac{\omega_i^2}{k_i^3} \int_{\mathbb{R}} \frac{\mathrm{Im}\left[B_{p_i}\left(\omega_i, \omega_2\right)\right]}{\left(2\xi_i\omega_i\right)^2 + \omega_2^2} \omega_2 \,\mathrm{d}\omega_2, \tag{17}$$

is recalled here with the current notations since it will be used for later comparison. It is made of (i) a quasi-static (background) response, obtained by dividing the third moment of the loading by the third power of the stiffness, and (ii) a bi-resonant contribution which is identifiable since it depends on the damping ratio ξ_i. This second component was coined *bi-resonant* in [24] since it corresponds to resonance in two of the three factors in the kernel $\mathcal{K}_{ijk}\left(\omega_1, \omega_2\right)$, defined in (15).

The main contribution of this paper is to extend this formulation to off-diagonal terms (cross-moments). In essence, we extend here (17) to the multi-modal response, like (12) extends (11) at second order. The early discussion in Section 5.1 will show that the extension to third order cross-moments has its share of surprises, and the derivation of the final expression for the multiple timescale approximation of the third moment will be detailed in the rest of Section 5.

Ultimately, once the third order cross-moments are obtained, it is possible to express the recombination of modal responses at third order and compute the third statistical moment of any structural response as follows

$$m_{3,x_n} = \mathbb{E}\left[x_n^3\right] = \sum_{i=1}^{n_\mathrm{m}} \sum_{j=1}^{n_\mathrm{m}} \sum_{k=1}^{n_\mathrm{m}} \phi_{ni}\phi_{nj}\phi_{nk} \mathbb{E}\left[q_i q_j q_k\right] = \sum_{i=1}^{n_\mathrm{m}} \sum_{j=1}^{n_\mathrm{m}} \sum_{k=1}^{n_\mathrm{m}} \phi_{ni}\phi_{nj}\phi_{nk} m_{3,q_{ijk}}. \tag{18}$$

By similarity with the Complete Quadratic Combination, this combination is called Complete Cubic Combination (CCC) as it includes all possible combinations of moments at third order. Again, we can isolate the contributions of the super-diagonal elements of the third moment matrix and write

$$m_{3,x_n} = \sum_{i=1}^{n_\mathrm{m}} \phi_{ni}^3 m_{3,q_i} + \sum_{i=1}^{n_\mathrm{m}} \sum_{j=1}^{n_\mathrm{m}} \sum_{\substack{k=1 \\ (j,k)\neq(i,i)}}^{n_\mathrm{m}} \phi_{ni}\phi_{nj}\phi_{nk} m_{3,q_{ijk}}. \tag{19}$$

When the triple summation is neglected, the resulting expression corresponds to the Cubic Root of the Sum of the Cubes (CRSC), which is similar to the Square Root of the Sum of the Squares combination. We emphasize that it is very tempting to drop the triple summation and consider the CRSC combination instead of the CCC. The saving is yet much more interesting than at second order. However, while it is possible to show that, at second order, the magnitude of the correlation coefficients of modal responses remain bounded to unity, in absolute value, such a bound does not exist at third order. Out-of-diagonal elements of the third moment matrix can therefore be larger, even much larger, than the diagonal ones. The Complete Cubic Combination makes therefore much more sense than the CRSC combination.

The practical usage of third statistical moments is revealed by means of the skewness coefficient, defined by

scaling the third moment by the third power of the standard deviation,

$$\gamma_{3,x_n} = \frac{m_{3,x_n}}{m_{2,x_n}^{3/2}}. \tag{20}$$

In the illustrations given at the end of the paper, the skewness coefficient of the displacements and bending moments in a bridge structure are computed. Two variants are shown, either keeping either discarding the cross-correlation sums in the estimation of the second and third moments of the structural responses. It is shown that the difference can be significant. This example serves as a motivation to derive simple expressions for the determination of the cross-moments of the modal responses $m_{3,q_{ijk}}$.

4. Specificities of the problem

4.1. Symmetries

The cross-bispectrum of stochastic (ergodic) processes $x_1(t)$, $x_2(t)$ and $x_3(t)$ can be computed as

$$B_{ijk}(\omega_1, \omega_2) = \lim_{T\to+\infty} \frac{1}{2\pi T} \mathbb{E}\left[X_i(\omega_1) X_j(\omega_2) \overline{X}_k(\omega_1+\omega_2)\right] \tag{21}$$

where $X_m(\omega) = \int_{-T/2}^{T/2} x_m(t) \mathrm{e}^{-\mathrm{i}\omega t} \mathrm{d}t$, $m \in \{i,j,k\}$ is the truncated Fourier transform of the process [1]. Since $X_m(-\omega) = \overline{X}_m(\omega)$ for $m \in \{i,j,k\}$,

$$B_{ijk}(-\omega_1, -\omega_2) = \overline{B}_{ijk}(\omega_1, \omega_2), \tag{22}$$

which indicates that the real part of the cross-bispectrum enjoys a central symmetry about $(\omega_1, \omega_2) = (0,0)$ while the imaginary part of the cross-bispectrum enjoys a central anti-symmetry about $(\omega_1, \omega_2) = (0,0)$. Thus, without any loss of generality, only half of the spectrum can be established, e.g. for $(\omega_1, \omega_2) \in \mathbb{R} \times \mathbb{R}^+$ and the real and imaginary parts of the bispectrum can be reconstructed everywhere else based on these symmetry properties, see Figure 2-b. Since the kernel $\mathcal{K}_{ijk}(\omega_1, \omega_2)$ has the same structure as the bispectrum, as indicated by its definition (15), it enjoys the same symmetry properties as the bispectrum,

$$\mathcal{K}_{ijk}(-\omega_1, -\omega_2) = \overline{\mathcal{K}}_{ijk}(\omega_1, \omega_2). \tag{23}$$

This is consistent with (14), where the kernel is expressed as a ratio of two bispectra and therefore needs to have the same symmetry properties.

A cross-bispectrum also exhibits some symmetry properties with respect to its indices, e.g. $B_{ijk}(\omega_1, \omega_2) = B_{jik}(\omega_2, \omega_1)$. This is easily demonstrated by swapping indices in the definition (21). This type of symmetry can be used to reconstruct the bispectrum for any permutation of the triplet (i,j,k) once it is known for any one of them. Moreover, the third-moment matrix $\mathbf{m}_3$ associated with this bispectrum has stronger symmetry properties with respect to its indices. Indeed, after integration, random processes become random variables, neither time nor frequency longer matters, and $\mathbf{m}_{3_{ijk}}$ is independent of any permutation of the triplet (i,j,k).

Super-diagonal elements of the bispectrum ($i = j = k$) feature additional symmetry conditions because of the commutativity of the product which can be exploited as soon as all three factors in (21) or (15) involve

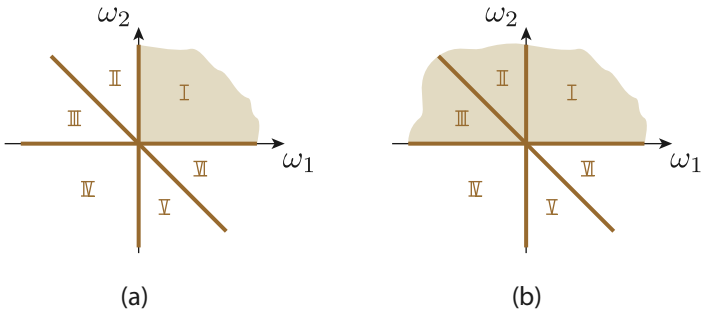

Figure 2: Illustration of the symmetry properties of bispectra (a) unilateral bispectrum ($i = j = k$), only one fourth of the frequency space is sufficient to reconstruct the bispectrum everywhere , (b) general case ($i \neq j \neq k$), one half of the frequency space is sufficient to reconstruct the bispectrum everywhere.

the same function. Consequently, the unilateral bispectrum ($i = j = k$) can be expressed on the quadrant $(\omega_1, \omega_2) \in \mathbb{R}^+ \times \mathbb{R}^+$ only, and the hexa-symmetry translated by

$$\begin{aligned} B_i(\omega_1, \omega_2) = \overline{B}_i(-\omega_1, \omega_1 + \omega_2) = B_i(-\omega_1 - \omega_2, \omega_1) = \overline{B}_i(-\omega_1, -\omega_2) \\ = B_i(\omega_1, -\omega_1 - \omega_2) = \overline{B}_i(\omega_1 + \omega_2, -\omega_1) \end{aligned} \tag{24}$$

can be used to reconstruct the bispectrum on the five other sextants, see Figure 2. In Figure 2-a, the roman numbers used to identify the sextants correspond to the six equations in (24), e.g. $B_i(\omega_1, \omega_2) = \overline{B}_i(-\omega_1, \omega_1 + \omega_2)$ can be used to reconstruct the bispectrum in the second sextant from the information available in the first one.

4.2. Real and Imaginary parts of the bispectra

Since we mostly focus on the integration of the cross-bispectra (of modal responses), only the central symmetry is exploited in the sequel. More precisely, and because it is expected that the modal responses are real stochastic processes, only the real part of $B_{q_{ijk}}(\omega_1, \omega_2)$ on the domain $(\omega_1, \omega_2) \in \mathbb{R} \times \mathbb{R}^+$ needs to be determined, without any loss of information. Because it is expressed as the product of two (possibly complex) quantities, rewriting (14) in the format

$$\mathrm{Re}\left\{B_{q_{ijk}}\right\} = \mathrm{Re}\left\{\mathcal{K}_{ijk}\right\} \mathrm{Re}\left\{B_{p_{ijk}}\right\} - \mathrm{Im}\left\{\mathcal{K}_{ijk}\right\} \mathrm{Im}\left\{B_{p_{ijk}}\right\} \tag{25}$$

shows that only the real (respectively imaginary) parts of $\mathcal{K}_{ijk}(\omega_1, \omega_2)$ and $B_{p_{ijk}}(\omega_1, \omega_2)$ need to be combined together.

4.3. Small numbers of the problem

This problem involves several small numbers. It is essential to explicitly formulate that these quantities are small and to do so, the small number $\varepsilon \ll 1$ is introduced. It is arbitrarily introduced in order to compare the various orders of magnitude of the different terms involved in the problem. Then, once simplifications and formal comparison of orders of magnitude are done, it will disappear from the final expression. Introducing this small quantity is standard approach in typical perturbation methods [40].

First, damping ratios are supposed to be small, $\xi_i \ll 1$, $\xi_j \ll 1$, $\xi_k \ll 1$. So they are written

$$\xi_i = \varepsilon\tilde{\xi}_i \quad ; \quad \xi_j = \varepsilon\tilde{\xi}_j \quad ; \quad \xi_k = \varepsilon\tilde{\xi}_k \tag{26}$$

where $\tilde{\xi}_i$, $\tilde{\xi}_j$ and $\tilde{\xi}_k$ are rescaled values of the damping ratio. They will be momentarily used instead of ξ_i, ξ_j and ξ_k so that the smallness of the damping ratios can be taken into account; after simplifications, (26) will be used again to express final results in terms of original problem parameters ξ_i, ξ_j and ξ_k. It is noticed that $\tilde{\xi}_i$, $\tilde{\xi}_j$ and $\tilde{\xi}_k$ can be as small as desired —for instance, they could be equal to zero in the undamped case—, but should be of order 1 at most. Indeed, if they were of order $1/\varepsilon$, the corresponding damping ratio would be of order 1, which is not consistent with the small damping assumption.

Assuming small damping implies that a typical frequency response function (3) can be expanded as

$$H_m(\omega) = \frac{1}{k_m}\frac{1}{1-\left(\frac{\omega}{\omega_m}\right)^2} - \frac{1}{k_m}\frac{2\mathrm{i}\varepsilon\tilde{\xi}_m\frac{\omega}{\omega_m}}{\left(1-\left(\frac{\omega}{\omega_m}\right)^2\right)^2} + \mathrm{ord}\left(\varepsilon^2\right) \tag{27}$$

for $m \in \{i, j, k\}$.

Second, as customary in wind engineering applications, the characteristic frequency content of the loading α is supposed to be much lower than the natural frequencies of the structure. In the sequel, we will focus on a generic cross-moment (i, j, k) with three natural frequencies ω_i, ω_j and ω_k, it is desired to state that

$$\alpha \ll \omega_i \quad ; \quad \alpha \ll \omega_j \quad ; \quad \alpha \ll \omega_k. \tag{28}$$

Alternatively, α is also small compared to the average of any combination of ω_i, ω_j and ω_k. For instance, to formalize that α is small with respect to the average value between ω_j and ω_k, noted $\hat{\omega}_{jk} = (\omega_j + \omega_k)/2$, we will later write

$$\alpha = \tilde{\alpha}\,\hat{\omega}_{jk}\varepsilon. \tag{29}$$

In this expression, $\tilde{\alpha}$ is a rescaled loading frequency of order 1 at most (for similar reasons as for $\tilde{\xi}_i$), $\hat{\omega}_{jk}$ is there to give units and ε is the (small) order of magnitude.

Last but not least, small relative differences of natural frequencies will also be explicitly stated in the rest of this document. For instance, to formalize that the natural frequencies in modes j and k are close to each other, we will refer to the difference

$$\frac{\omega_k - \omega_j}{\omega_k + \omega_j} = \frac{\omega_k - \omega_j}{2\hat{\omega}_{jk}} = \varepsilon\tilde{\delta}_{jk} \tag{30}$$

where $\tilde{\delta}_{jk}$ refers to a rescaled relative distance between ω_j and ω_k. While the first two assumptions (26) and (29) are valid throughout the document, small relative differences of natural frequencies as expressed in (30) will only be used occasionally whenever such condition is formulated.

5. Multiple Timescale Spectral Analysis

As motivated earlier, the out-of-diagonal elements of the third moment matrix of modal responses, $m_{3,q_{ijk}}$, are essential to the Complete Cubic Combination. They are explicitly obtained by the integration of the

corresponding cross-bispectrum, see (16). In this Section, the Multiple Timescale Spectral Analysis is specialized to the computation of that specific integral. It is an approximate method, but since it is semi-analytical, it is much faster.

5.1. General overview of the problem

The peaks in the bispectrum such as those visible in the sketch of Figure 1 are located at the intersections of crests which correspond themselves to the locations of poles in the factors composing the kernel $\mathcal{K}_{ijk}$ or the bispectrum of the loading. More specifically the kernel $\mathcal{K}_{ijk}$ exhibits three pairs of crests, each pair being associated with each factor composing the kernel $\mathcal{K}_{ijk}$, see (15). Similarly, the bispectrum of the loading has three main crests, intersecting at the origin; they are clearly visible in Figure 1-b.

In the most general case, the cross-bispectrum of the response can exhibit up to 25 different peaks corresponding to the intersections, in the (ω_1, ω_2) −plane of the different crest lines in the various factors composing the bispectrum, see Figure 3-a. Since the Multiple Timescale Spectral Analysis consists in the successive focus on each peak in the response, a systematic application of the method would be tedious. Central symmetry can be invoked first to reduce the problem to a half-plane where only 13 peaks can be considered. They are represented and labelled in Figure 3-a. These peaks are classified in three different categories:

- the background peak (#1) is unique; it is located near the origin, where the three factors in the kernel are in the quasi-static regime (ω_1 and ω_2 much smaller than the natural frequencies);
- the mixed background-resonant peaks (#2, #3, $\cdots$,#7), where one or two of the three factors in the kernel are in the resonant regime (either ω_1, ω_2 or $\omega_1 + \omega_2$ corresponds to the natural frequency) and where the bispectrum of the loading is important, meaning that these peaks are also located along the crest where the bispectrum of the loading is important (thick brown lines);
- the bi- and tri-resonant peaks (#8, #9, $\cdots$,#13) where two or three factors in the kernel are in the resonant regime. They correspond to the intersections of the dashed lines in Figure 3. Depending on the specific values of the three natural frequencies, these peaks are bi- or tri-resonant. In the two cases shown in Figures 3, only bi-resonance is illustrated since, only two dashed lines cross at the same time. However, when $\omega_k = \omega_i + \omega_j$, the three peaks labelled #8, #9 and #13, located in the yellow triangle, merge. This gives rise to tri-resonance. This phenomenon is only observable for cross-moments for which one frequency is the sum of two others (or one is the double as another).

The type and coordinates of each peak are also given in Table 1.

Beside usage of symmetry, the solution of the problem can be drastically simplified by analyzing the orders of magnitude of the different contributions to the cross-moment that each peak can offer. For instance, from previous works [24], it is known that the unilateral bispectrum of the modal response, see Figure 3-b, has a background component (#1) and six major mixed background-resonant peaks (#2,3,8, #6,7,10 and #4,5,9) while the bi-resonant peaks (#11, #12, #13) can be neglected.

A rigorous analysis of the order of magnitude of each peak, in the more general case of the cross-moment, has been carried out. It is summarized in Table 2. For each peak, we indicate the order of magnitude of

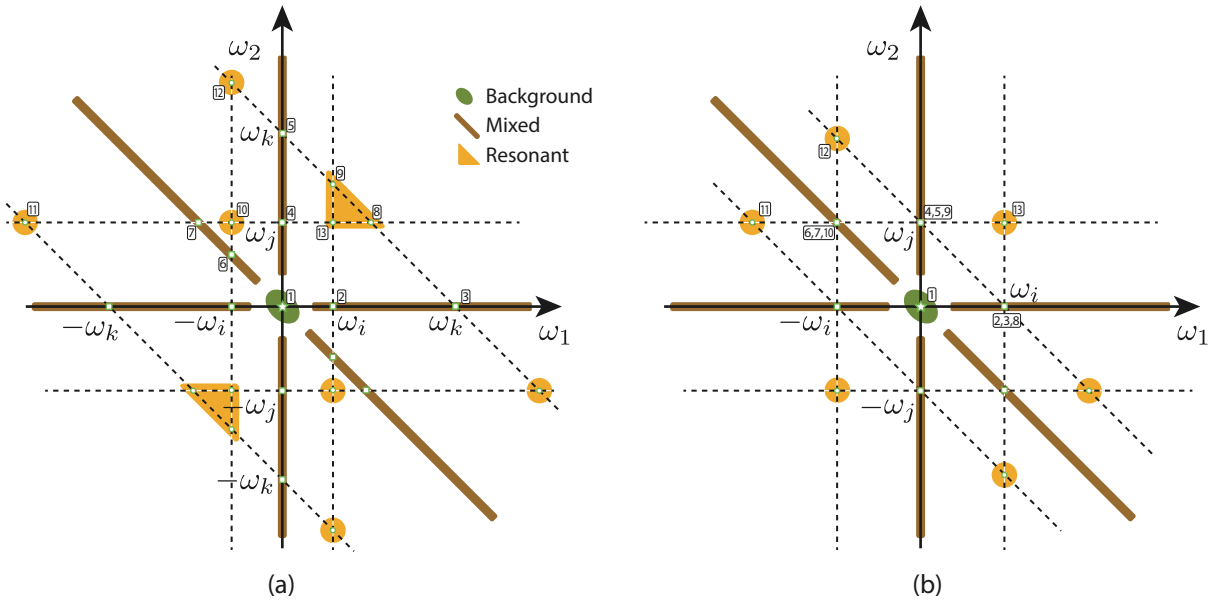

Figure 3: Location and classification of the different peaks in a cross bispectrum (a) general case with $\omega_i \neq \omega_j \neq \omega_k$, (b) particular case with $\omega_i = \omega_j = \omega_k$.

		Peak No.	(ω_1, ω_2)	$\omega_1 + \omega_2$
●	Background	#1	$(0, 0)$	0
╲	Mixed B-R	#2	$(\omega_i, 0)$	ω_i
		#3	$(\omega_k, 0)$	ω_k
		#4	$(0, \omega_j)$	ω_j
		#5	$(0, \omega_k)$	ω_k
		#6	$(-\omega_i, \omega_i)$	0
		#7	$(-\omega_j, \omega_j)$	0
◣	bi-/tri-resonant	#8	$(\omega_k - \omega_j, \omega_j)$	ω_k
		#9	$(\omega_i, \omega_k - \omega_i)$	ω_k
		#10	$(-\omega_i, \omega_j)$	$\omega_j - \omega_i$
		#11	$(-\omega_k - \omega_j, \omega_j)$	$-\omega_k$
		#12	$(-\omega_i, \omega_i + \omega_k)$	ω_k
		#13	(ω_i, ω_j)	$\omega_i + \omega_j$

Table 1: Location and classification of the 13 peaks located in the upper half frequency space.

No.	$X_p(\omega_1)$	$X_p(\omega_2)$	$X_p(\omega_1+\omega_2)$	$H_i(\omega_1)$	$H_j(\omega_2)$	$\overline{H}_k(\omega_1+\omega_2)$	$B_{ijk}(\omega_1,\omega_2)$	condition
#1	$1/\varepsilon$	$1/\varepsilon$	$1/\varepsilon$	1	1	1	$1/\varepsilon^3$	-
#2	1	$1/\varepsilon$	1	$1/\varepsilon$	1	$\lceil 1/\varepsilon \rceil$	$1/\varepsilon^3$	$\omega_i \simeq \omega_k$
#3	1	$1/\varepsilon$	1	$\lceil 1/\varepsilon \rceil$	1	$1/\varepsilon$	$1/\varepsilon^3$	$\omega_i \simeq \omega_k$
#4	$1/\varepsilon$	1	1	1	$1/\varepsilon$	$\lceil 1/\varepsilon \rceil$	$1/\varepsilon^3$	$\omega_j \simeq \omega_k$
#5	$1/\varepsilon$	1	1	1	$\lceil 1/\varepsilon \rceil$	$1/\varepsilon$	$1/\varepsilon^3$	$\omega_j \simeq \omega_k$
#6	1	1	$1/\varepsilon$	$1/\varepsilon$	$\lceil 1/\varepsilon \rceil$	1	$1/\varepsilon^3$	$\omega_i \simeq \omega_j$
#7	1	1	$1/\varepsilon$	$\lceil 1/\varepsilon \rceil$	$1/\varepsilon$	1	$1/\varepsilon^3$	$\omega_i \simeq \omega_j$
#8	$\lceil 1/\varepsilon \rceil$	1	1	$\lceil 1/\varepsilon \rceil$	$1/\varepsilon$	$1/\varepsilon$	$1/\varepsilon^3$	$\omega_i \simeq \omega_k - \omega_j$
#9	1	$\lceil 1/\varepsilon \rceil$	1	$1/\varepsilon$	$\lceil 1/\varepsilon \rceil$	$1/\varepsilon$	$1/\varepsilon^3$	$\omega_j \simeq \omega_k - \omega_i$
#10	1	1	$\lceil 1/\varepsilon \rceil$	$1/\varepsilon$	$1/\varepsilon$	$\lceil 1/\varepsilon \rceil$	$1/\varepsilon^3$	$\omega_k \simeq \omega_j - \omega_i$
#11	ε	1	1	$\lceil 1/\varepsilon \rceil$	$1/\varepsilon$	$1/\varepsilon$	$(1/\varepsilon^2)$	$\omega_i \simeq \omega_k - \omega_j$
#12	1	ε	1	$1/\varepsilon$	$\lceil 1/\varepsilon \rceil$	$1/\varepsilon$	$(1/\varepsilon^2)$	$\omega_j \simeq \omega_k - \omega_i$
#13	1	1	ε	$1/\varepsilon$	$1/\varepsilon$	$\lceil 1/\varepsilon \rceil$	$(1/\varepsilon^2)$	$\omega_k \simeq \omega_j - \omega_i$

Table 2: Relative orders of magnitude of the different factors composing the bispectrum of the response. The symbol $\lceil \cdot \rceil$ is used to indicate that the quantities are at most of a given order. Conditions to reach this order of magnitude are given in the last column.

each of the six factors composing the bispectrum of the response ($X_p(\omega_1)$, $X_p(\omega_2)$, $\bar{X}_p(\omega_1+\omega_2)$, $H_i(\omega_1)$, $H_j(\omega_2)$, $\bar{H}_k(\omega_1+\omega_2)$). In order to simplify notations, indices i, j and k are dropped in the truncated Fourier transform of the modal loads $X_p(\cdot)$. The relative orders of magnitude of $X_p(\omega)$ are: $1/\varepsilon$ for $|\omega| \sim \alpha$, 1 for $|\omega| \sim \{\omega_i, \omega_j, \omega_k\}$, and ε for $|\omega| \sim 2\{\omega_i, \omega_j, \omega_k\}$. This stems from the fact that $\alpha \sim \varepsilon$ and is fully consistent with the fact that the bispectrum of the loading assumes large values along the three ridges represented by brown thick lines in Figure 3. Then, just by considering the values of ω_1, ω_2 and $\omega_1+\omega_2$ of each peak (see Table 1), the orders of magnitude of $X_p(\omega_1)$, $X_p(\omega_2)$, $\bar{X}_p(\omega_1+\omega_2)$ can be established. They are given in Table 2 (first three columns). It is seen that all three factors are of order $1/\varepsilon$ for the background peak (#1), while only one of the three is of order $1/\varepsilon$ for the mixed peaks, along the thick brown lines (#2, #3, #4, #5, #6, #7), and at most one factor is large, upon condition, for the resonant peaks (#8, #9, #10, #11, #12). For instance, at the location of peak #8, $\omega_1 = \omega_k - \omega_j$ (see Table 1) and $X_p(\omega_1) = X_p(\omega_k - \omega_j)$. So, depending on whether $|\omega_k - \omega_j| \sim \alpha$, $|\omega_k - \omega_j| \sim \{\omega_i, \omega_j, \omega_k\}$ or $|\omega_k - \omega_j| \sim 2\{\omega_i, \omega_j, \omega_k\}$, the order of magnitude of that factor at the location of peak #8 can take very different values. The most important one, is when $|\omega_k - \omega_j| \sim \alpha$, in which case, $X_p(\omega_1) \sim 1/\varepsilon$ and this peak is potentially (and conditionally) large. This condition is schematically represented by the symbol $\lceil 1/\varepsilon \rceil$ in Table 2, meaning that at most $X_p(\omega_1) \sim 1/\varepsilon$ for peak #8.

The same exercise is repeated for the frequency response functions $H_i(\omega_1)$, $H_j(\omega_2)$ and $\bar{H}_k(\omega_1+\omega_2)$. In this case, it is noticed that the relative order of magnitude of $H_m(\omega)$ is: 1 for $|\omega| \ll \omega_m$, $1/\varepsilon$ for $|\omega| \sim \omega_m$ (resonance, the response is inversely proportional to damping $\xi_m \sim \varepsilon$), and ε for $|\omega| \gg \omega_m$. In particular, the three factors are of order 1 for the background peak (#1) since they correspond to the quasi-static regime. The mixed peaks (#2, #3, #4, #5, #6, #7) have one resonance for sure and possibly a second one. For instance, for

peak #2, $H_i(\omega_1) = H_i(\omega_i) \sim 1/\varepsilon$ is resonant, $H_j(\omega_2) = H_j(0) \sim 1$ is quasi-static and $\bar{H}_k(\omega_1 + \omega_2) = \bar{H}_k(\omega_i)$, which is resonant under the condition $\omega_i \simeq \omega_k$. For this reason it is also noted $\lceil 1/\varepsilon \rceil$ in Table 2. Bi- and tri-resonant peaks (#8, #9, #10, #11, #12) correspond to resonance in at least two of the three frequency response functions, and possibly three upon condition.

Finally, the order of magnitude of the contribution of each peak in the response bispectrum can be established by combining the orders of magnitude of the six factors. They are reported in column with heading $B_{ijk}(\omega_1, \omega_2)$, followed by the condition to reach the largest order of magnitude. Since the extent of each peak in the (ω_1, ω_2) plane is of order ε^2 for each of them (it is α^2 for the background and ξ_m^2 for the resonance), comparison of the value of the bispectrum is sufficient to sort out the different peaks according to their importance. From this, it is seen that:

- the order of magnitude of the response bispectrum in the background component is always $1/\varepsilon^3$,
- the other contributions might therefore be neglected if they do not reach the same order of magnitude,
- the six mixed peaks (#2, ..., #7) could contribute with the same order of magnitude, as soon as one of the following conditions is met, $\omega_i \simeq \omega_k$, $\omega_j \simeq \omega_k$ or $\omega_i \simeq \omega_j$. If all three conditions are met, $\omega_i \simeq \omega_j \simeq \omega_k$ all six peaks contribute. In the particular case where $\omega_i = \omega_j = \omega_k$ (e.g. diagonal elements of $\mathbf{m}_3$), they all contribute equally;
- three out of the six resonant peaks (#8, #9, #10) could also contribute with the same order of magnitude. There are two ways to do so. The first one is to have an important background, under the conditions: $\omega_i \simeq \omega_k$, $\omega_j \simeq \omega_k$ or $\omega_i \simeq \omega_j$, in which case they actually turn to be mixed contributions (#4,5,8 merge; #2,3,9 merge or #6,#7,#10 merge). This case is covered by the previous item. The second way to have a leading order contribution of peaks (#8, #9, #10) is under one of the following conditions $\omega_i \simeq \omega_k - \omega_j$, $\omega_j \simeq \omega_k - \omega_i$, or $\omega_k \simeq \omega_j - \omega_i$. In this case, resonance takes place in each mode (tri-resonance) and the three peaks located in the yellow triangle in Figure 3-a collapse to the same point;
- the three other resonant peaks (#11, #12, #13) indicated by isolated yellow circles in Figure 3 have a smaller order of magnitude and can always be neglected.

In the following, the solution is simplified by noticing that $\mathbf{m}_{3,q_{ijk}}$ is independent of any permutation of the triplet (i, j, k). Without any loss of generality, it is therefore assumed that $\omega_i \leq \omega_j \leq \omega_k$. A specific focus will be given, in the following subsections, to the three different components that can arise in such circumstances, i.e. (i) the background component, near the origin, (ii) the mixed background-resonant peaks located along the axes where the bispectrum of loading is important (brown lines), they will be studied only in the cases where $\omega_i \simeq \omega_k$, $\omega_j \simeq \omega_k$ or $\omega_i \simeq \omega_j$; otherwise they would yield smaller contributions, (iii) the tri-resonant peaks located in the neighborhood of the yellow triangles in Figure 3 whenever they collapse to a very small area, of the order of magnitude of the damping ratio. Considering that $\omega_i \leq \omega_j \leq \omega_k$, the only way to reach this condition is to have $\omega_k \simeq \omega_i + \omega_j$. It is already underlined that this latter contribution is totally new and could not have been observed in the single degree-of-freedom case, for which the condition $\omega_k \simeq \omega_i + \omega_j$ cannot be met. These three contributions are derived in detail in the following three subsections.

5.2. Contribution 1: background

The general theory of the Multiple Timescale Spectral Analysis [31] recommends to start with the background component, which is easily identifiable. In our case, it is readily obtained by approximating the kernel as $\mathcal{K}_{ijk}(\omega_1, \omega_2) = 1/k_i k_j k_k$ so that (16) yields

$$m_{3,b_{ijk}} = \iint_{\mathbb{R}^2} \frac{1}{k_i k_j k_k} B_{p_{ijk}}(\omega_1, \omega_2)\, \mathrm{d}\omega_1 \mathrm{d}\omega_2 = \frac{m_{3,f_{ijk}}}{k_i k_j k_k}, \tag{31}$$

which indicates that the third moment of the background response is directly obtained from the third moment of modal loads. This naturally extends to cross-moments the same logic [24] as for the super-diagonal element $(i = j = k)$.

This first component can then be subtracted from the original expression (16), leaving the residual

$$m_{ijk} - m_{3,b_{ijk}} = \iint_{\mathbb{R}^2} \hat{\mathcal{K}}_{ijk}(\omega_1, \omega_2)\, B_{p_{ijk}}(\omega_1, \omega_2)\, \mathrm{d}\omega_1 \mathrm{d}\omega_2 \tag{32}$$

where $\hat{\mathcal{K}}_{ijk}(\omega_1, \omega_2) = \mathcal{K}_{ijk}(\omega_1, \omega_2) - \frac{1}{k_i k_j k_k}$. In this integrand, there is no longer any peak in the neighborhood of the origin and it is possible to focus on the other two contributions.

5.3. Contribution 2: mixed background/bi-resonant

Mixed contributions are located along the ridges of the bispectrum of loading. There are 12 peaks along those ridges where the kernel $\mathcal{K}(\omega_1, \omega_2)$ takes large values in the neighborhood of resonance peaks. Half of them, located in the upper half plane are labelled #2, #3,$\cdots$, #7 in Figure 3-a. In the specific case depicted in Figure 3-a, all three natural frequencies are relatively well distinct (with respect to the width of resonance peaks) so that they correspond to mono-resonance. In case two (at least) of the three natural frequencies are close to each other, bi-resonance takes place along a ridge of important background response, as discussed earlier. Some peaks then collapse to a single point, as illustrated in Figure 3-b for $\omega_i = \omega_j = \omega_k$.

The determination of the mixed contribution is therefore only relevant for the local contribution in the neighborhood of (a) $(\omega_1, \omega_2) = (\omega_i, 0)$ with $\omega_k \simeq \omega_i$ (peaks labelled #2 and #3), (b) $(\omega_1, \omega_2) = (0, \omega_j)$ with $\omega_k \simeq \omega_j$ (peaks labelled #4 and #5), (c) $(\omega_1, \omega_2) = (-\omega_i, \omega_i)$ with $\omega_j \simeq \omega_i$ (peaks labelled #6 and #7). The second one of these contributions will be treated in detail and the other two will be obtained by circular symmetry.

When $\omega_j \simeq \omega_k$, the two peaks #4 and #5 are close to each other. In the limit case, $\omega_j = \omega_k$, they merge. In order to formalize this, we explicitly state that the relative distance between the two natural frequencies has the same order of magnitude as the width of the resonance peaks (the damping ratio, of order ε),

$$\omega_j = \hat{\omega}_{jk}(1 - \varepsilon\delta), \quad \omega_k = \hat{\omega}_{jk}(1 + \varepsilon\delta) \tag{33}$$

where $\hat{\omega}_{jk} = (\omega_j + \omega_k)/2$ is the average natural frequency. The change of variables (33) maps (ω_j, ω_k) onto $(\hat{\omega}_{jk}, \delta)$. Substitution of these definitions in $\omega_k - \omega_j$ shows that $2\varepsilon\delta = (\omega_k - \omega_j)/\hat{\omega}_{jk}$, so that δ can be seen as a relative difference of natural frequencies.

The standard technique of the Multiple Timescale Spectral Analysis [31] can now be applied. The width of the considered peak in the ω_1-direction is the small frequency $\alpha \sim \varepsilon$, which is arbitrarily written $\alpha = \tilde{\alpha}\,\hat{\omega}_{jk}\varepsilon$ to indicate that the characteristic frequency of the loading is small with respect to the natural frequencies. The dimensionless parameter $\tilde{\alpha}$ is of order 1 at most, and it is just temporarily introduced to be rigorous; it will be soon replaced back by α again. The order of magnitude of the width of the peak in the ω_2-direction is $\hat{\omega}_{jk}\varepsilon$ because the damping ratio is of order ε, see Section 4.3. So the stretched coordinates η_1 and η_2 necessary to focus on this peak are naturally chosen as

$$\omega_1 = \tilde{\alpha}\,\hat{\omega}_{jk}\varepsilon\,\eta_1 \quad \text{and} \quad \omega_2 = \hat{\omega}_{jk}\,(1+\varepsilon\eta_2)\,. \tag{34}$$

They are centered and normalized in the sense that, for $\eta_1 = \eta_2 = 0$, $(\omega_1, \omega_2) = (0, \hat{\omega}_{jk})$, and $(\eta_1, \eta_2) \sim 1$. With these stretched coordinates, we have

$$\frac{\omega_1}{\omega_i} = \frac{\tilde{\alpha}\hat{\omega}_{jk}\varepsilon\,\eta_1}{\omega_i} \quad ; \quad \frac{\omega_2}{\omega_j} = \frac{\hat{\omega}_{jk}\,(1+\varepsilon\eta_2)}{\hat{\omega}_{jk}\,(1-\varepsilon\delta)} \sim 1+\varepsilon\,(\eta_2+\delta) \quad ; \quad \frac{\omega_1+\omega_2}{\omega_k} = \frac{\tilde{\alpha}\varepsilon\,\eta_1+(1+\varepsilon\eta_2)}{1+\varepsilon\delta} \sim 1+\varepsilon\,(\tilde{\alpha}\,\eta_1+\eta_2-\delta) \tag{35}$$

so that substitution in (27) yields after expansion for small ε and truncation at leading order,

$$H_i\,(\omega_1) = \frac{1}{k_i} \quad ; \quad H_j\,(\omega_2) = \frac{1}{k_j}\frac{1}{2\varepsilon}\frac{-1}{\eta_2+\delta-\mathrm{i}\tilde{\xi}_j} \quad ; \quad \bar{H}_k\,(\omega_1+\omega_2) = \frac{1}{k_k}\frac{1}{2\varepsilon}\frac{-1}{\tilde{\alpha}\eta_1+\eta_2-\delta+\mathrm{i}\tilde{\xi}_k}. \tag{36}$$

This indeed indicates resonance in two of the three factors (j and k), hence, bi-resonance. The kernel reads

$$\mathcal{K}_{ijk}\,(\omega_1\,(\eta_1)\,,\omega_2\,(\eta_2)) = \frac{1}{k_i k_j k_k}\frac{1}{4\varepsilon^2}\frac{1}{\eta_2+\delta-\mathrm{i}\tilde{\xi}_j}\frac{1}{\tilde{\alpha}\eta_1+\eta_2-\delta+\mathrm{i}\tilde{\xi}_k} \tag{37}$$

plus higher order terms in $1/\varepsilon$ which are neglected. It is also noticed that the residual $\hat{\mathcal{K}}_{ijk}\,(\omega_1,\omega_2)$ assumes the same expansion as the kernel and, as a consequence, $\hat{\mathcal{K}}_{ijk}\,(\omega_1,\omega_2)$ can be equally replaced by $\mathcal{K}_{ijk}\,(\omega_1,\omega_2)$. The bispectrum of the loading, in that specific area of the frequency space, is

$$B_{p_{ijk}}\,(\tilde{\alpha}\hat{\omega}_{jk}\varepsilon\,\eta_1,\hat{\omega}_{jk}\,(1+\varepsilon\eta_2)) = B_{p_{ijk}}\,(\tilde{\alpha}\hat{\omega}_{jk}\varepsilon\,\eta_1,\hat{\omega}_{jk}) + \varepsilon\eta_2\hat{\omega}_{ik}\partial_{\omega_2}B_{p_{ijk}}\,(\tilde{\alpha}\hat{\omega}_{jk}\varepsilon\,\eta_1,\hat{\omega}_{jk}) + \mathrm{ord}\left(\varepsilon^2\right). \tag{38}$$

It is assumed that the gradient $\partial_{\omega_2}B_{p_{ijk}}$ of the bispectrum of loading along ω_2 is of order 1 at most in the neighborhood of the bi-resonant peak located at $(\omega_1,\omega_2) = (0,\hat{\omega}_{jk})$. This hypothesis is very similar to that formulated in the classical background/resonant decomposition [27, 38]. Alternative formulations do exist otherwise [31] but are not considered here; they are not required in case of wind loading, which is here the target application. We also underline that the conjugate gradient $\partial_{\omega_1}B_{p_{ijk}}$ might be large close to the peak at $(0,\hat{\omega}_{jk})$ so that no assumption is made with respect to that slow timescale.

Considering that the bispectrum of loading is slightly sensitive to changes in η_2, meaning that the second term in (38) is of higher order, the bispectrum of loading is approximated by $B_{p_{ijk}}\,(\tilde{\alpha}\hat{\omega}_{jk}\varepsilon\,\eta_1,\hat{\omega}_{jk})$ and substitution of (37) and (38) into (32) shows that the contribution to the third central moment, coming from the bi-resonant peaks #4 and #5 can be worked out as follows,

$$\mathcal{I}_{3,r_{jk}} = \frac{1}{k_i k_j k_k} \frac{1}{4\varepsilon^2} \iint\limits_{\mathbb{R}^2} \frac{B_{p_{ijk}}\left(\tilde{\alpha}\hat{\omega}_{jk}\varepsilon\,\eta_1, \hat{\omega}_{jk}\right)}{\left(\eta_2 + \delta - \mathrm{i}\tilde{\xi}_j\right)\left(\tilde{\alpha}\eta_1 + \eta_2 - \delta + \mathrm{i}\tilde{\xi}_k\right)} \tilde{\alpha}\hat{\omega}_{jk}\varepsilon \mathrm{d}\eta_1 \hat{\omega}_{jk}\varepsilon \mathrm{d}\eta_2$$
$$= \frac{1}{k_i k_j k_k} \frac{\pi\hat{\omega}_{jk}}{2\varepsilon} \int\limits_{\mathbb{R}} \frac{B_{p_{ijk}}\left(\tilde{\alpha}\hat{\omega}_{jk}\varepsilon\,\eta_1, \hat{\omega}_{jk}\right)}{\tilde{\xi}_j + \tilde{\xi}_k - \mathrm{i}\,\tilde{\alpha}\,\eta_1 + 2\mathrm{i}\delta} \tilde{\alpha}\hat{\omega}_{jk}\varepsilon \mathrm{d}\eta_1. \tag{39}$$

Using the reverse change of coordinates $\omega_1 = \tilde{\alpha}\,\hat{\omega}_{jk}\varepsilon\,\eta_1$, and noticing that $\omega_k - \omega_j = 2\hat{\omega}_{jk}\varepsilon\delta$, we can now return to the original frequency space

$$\mathcal{I}_{3,r_{jk}} = \frac{1}{k_i k_j k_k} \frac{\pi\hat{\omega}_{jk}^2}{2} \int\limits_{\mathbb{R}} \frac{B_{p_{ijk}}\left(\omega_1, \hat{\omega}_{jk}\right) \mathrm{d}\omega_1}{\left(\xi_j + \xi_k\right)\hat{\omega}_{jk} + \mathrm{i}\left(\omega_k - \omega_j - \omega_1\right)}. \tag{40}$$

At the same time we could also eliminate $\tilde{\alpha}$ as well as the arbitrary and small parameter ε that had been introduced to formalize the smallness of some quantities in this problem. This expression is therefore a local contribution to the third cross-moment in the neighborhood of peaks labelled #4 and #5 in Figure 3. It is remarkable that, instead of the two-fold integral that would be necessary in principle, the local contribution is obtained by integrating along a single line. This translates into massive computational savings in the analysis of large structures because of the heavy computational cost of the evaluation of the bispectrum of modal loads, obtained by projection.

Equation (40) involves complex quantities, both in $B_{p_{ijk}}\left(\omega_1, \hat{\omega}_{jk}\right)$ and in the denominator. The exact result of this integral might not be real-valued. This is a consequence of the approximation that has been made to obtain this simplified expression. In order to make sure the result of the integral is well real-valued, the imaginary part can just be dropped, which gives

$$m_{3,r_{jk}} = 2\,\mathcal{I}_{3,r_{jk}} = \frac{\pi\hat{\omega}_{jk}^2}{k_i k_j k_k} \int\limits_{\mathbb{R}} \mathrm{Re}\left[\frac{B_{p_{ijk}}\left(\Omega, \hat{\omega}_{jk}\right)}{\left(\xi_j + \xi_k\right)\hat{\omega}_{jk} + \mathrm{i}\left(\omega_k - \omega_j - \Omega\right)}\right] \mathrm{d}\Omega, \tag{41}$$

where multiplication by 2 accounts for the symmetrically located peaks. All in all, $m_{3,r_{jk}}$ is the contribution to the third moment coming from the interaction between resonance peaks in modes j and k.

We are now in a position to review the conditions under which this contribution to the third cross-moment is significant. A first necessary condition for this interaction between modes j and k to be significant is that the denominator in (41) be small, which is the case when

$$\Omega \simeq \omega_k - \omega_j. \tag{42}$$

A second necessary condition is that the numerator $B_{p_{ijk}}\left(\Omega, \hat{\omega}_{jk}\right)$ be large, which happens to be the case in two distinct conditions:

1. $|\Omega| \sim \alpha$, which is a small frequency (remember $\alpha \ll \hat{\omega}_{jk}$); and so, combining with (42), $|\omega_k - \omega_j|$ should be small ($|\omega_k - \omega_j| \sim \alpha$) for the contribution $m_{3,r_{jk}}$ to be significant, or,
2. $\Omega \sim -\hat{\omega}_{jk}$, which, together with the condition (42) yields $\omega_k - \omega_j \sim -\hat{\omega}_{jk}$, i.e. $\omega_k \sim \frac{1}{3}\omega_j$.

The first case, $\omega_k - \omega_j \ll \hat{\omega}_{jk}$ precisely corresponds to the hypothesis that has been made, the small relative difference between natural frequencies ω_j and ω_k. The second case however does not correspond to the formulated hypothesis. It can be seen as a spurious contribution to the third moment but it is never activated

as long as care is taken to order the natural frequencies. Indeed, the condition $\omega_k \sim \frac{1}{3}\omega_j$ can never be met if $\omega_k \geq \omega_j$. As a conclusion, the proposed formulation for the jk-biresonant contribution $m_{3,r_{jk}}$, given in (41), is only significant when the natural frequencies are relatively close to each other.

The same contributions $m_{3,r_{ij}}$ and $m_{3,r_{ik}}$ exist for the possible interactions between modes i and j, and modes i and k. They are obtained with a very similar procedure whose details are skipped and which finally yields

$$m_{3,r_{ik}} = \frac{\pi\hat{\omega}_{ik}^2}{k_i k_j k_k} \int\limits_{\mathbb{R}} \mathrm{Re}\left[\frac{B_{p_{ijk}}\left(\hat{\omega}_{ik}, \Omega\right)}{\left(\xi_i + \xi_k\right)\hat{\omega}_{ik} + \mathrm{i}\left(\omega_k - \omega_i - \Omega\right)}\right] \mathrm{d}\Omega, \tag{43}$$

$$m_{3,r_{ij}} = \frac{\pi\hat{\omega}_{ij}^2}{k_i k_j k_k} \int\limits_{\mathbb{R}} \mathrm{Re}\left[\frac{B_{p_{ijk}}\left(-\hat{\omega}_{ij} + \frac{\Omega}{2}, \hat{\omega}_{ij} + \frac{\Omega}{2}\right)}{\left(\xi_i + \xi_j\right)\hat{\omega}_{ij} + \mathrm{i}\left(\omega_i - \omega_j + \Omega\right)}\right] \mathrm{d}\Omega. \tag{44}$$

5.4. Contribution 3: tri-resonant

A tri-resonant contribution occurs when any one of the three natural frequencies is close to the sum of two others. Owing to the sorting condition $\omega_i \leq \omega_j \leq \omega_k$, this condition translates into ω_k close to $\omega_i + \omega_j$, which is made explicit by writing $\omega_k = \left(\omega_i + \omega_j\right)\left(1 + \varepsilon\delta\right)$. Two stretched coordinates $\omega_1 = \omega_i\left(1 + \varepsilon\eta_1\right)$, $\omega_2 = \omega_j\left(1 + \varepsilon\eta_2\right)$ are introduced to zoom in the peak located at $\left(\omega_1, \omega_2\right) = \left(\omega_i, \omega_j\right)$. Noticing that

$$\frac{\omega_1}{\omega_i} \sim 1 + \varepsilon\eta_1 \quad ; \quad \frac{\omega_2}{\omega_j} \sim 1 + \varepsilon\eta_2 \quad ; \quad \frac{\omega_1 + \omega_2}{\omega_k} \sim \frac{\omega_i}{\omega_i + \omega_j}\left(1 + \varepsilon\eta_1 - \varepsilon\delta\right) + \frac{\omega_j}{\omega_i + \omega_j}\left(1 + \varepsilon\eta_2 - \varepsilon\delta\right), \tag{45}$$

substitution in (27) yields after expansion for small ε and truncation at leading order,

$$H_i\left(\omega_1\right) = \frac{1}{k_i}\frac{1}{2\varepsilon}\frac{-1}{\eta_1 - \mathrm{i}\tilde{\xi}_i} \quad ; \quad H_j\left(\omega_2\right) = \frac{1}{k_j}\frac{1}{2\varepsilon}\frac{-1}{\eta_2 - \mathrm{i}\tilde{\xi}_j} \quad ; \quad \bar{H}_k\left(\omega_1 + \omega_2\right) = \frac{1}{k_k}\frac{1}{2\varepsilon}\frac{-1}{-\frac{\omega_i\eta_1 + \omega_j\eta_2}{\omega_i + \omega_j} + \delta - \mathrm{i}\tilde{\xi}_k}. \tag{46}$$

so that the kernel is locally approximated by

$$\mathcal{K}\left(\eta_1, \eta_2\right) = \frac{1}{k_i k_j k_k}\frac{1}{8\varepsilon^3}\frac{1}{-\eta_1 + \mathrm{i}\tilde{\xi}_i}\frac{1}{-\eta_2 + \mathrm{i}\tilde{\xi}_j}\frac{1}{-\frac{\omega_i\eta_1 + \omega_j\eta_2}{\omega_i + \omega_j} + \delta - \mathrm{i}\tilde{\xi}_k}. \tag{47}$$

Observing that the bispectrum of the loading does not significantly change over the width of the tri-resonance peak, and that the jacobian of the stretching is $\varepsilon^2\omega_i\omega_j$, the contribution to the third moment of the modal response is

$$\mathcal{I}_{\mathrm{t}} = \frac{B_{p_{ijk}}\left(\omega_i, \omega_j\right)}{k_i k_j k_k} \iint\limits_{\mathbb{R}^2} \frac{1}{8\varepsilon^3}\frac{1}{-\eta_1 + \mathrm{i}\tilde{\xi}_i}\frac{1}{-\eta_2 + \mathrm{i}\tilde{\xi}_j}\frac{1}{-\frac{\omega_i\eta_1 + \omega_j\eta_2}{\omega_i + \omega_j} + \delta - \mathrm{i}\tilde{\xi}_k}\varepsilon^2\omega_i\omega_j \mathrm{d}\eta_1 \mathrm{d}\eta_2. \tag{48}$$

After some standard calculus, this double integral is evaluated as

$$\mathcal{I}_{\mathrm{t}} = \frac{B_{p_{ijk}}\left(\omega_i, \omega_j\right)}{k_i k_j k_k}\frac{\pi^2}{2\varepsilon}\frac{\omega_i\omega_j}{-\delta + \mathrm{i}\frac{\omega_i\left(\tilde{\xi}_i + \tilde{\xi}_k\right) + \omega_j\left(\tilde{\xi}_j + \tilde{\xi}_k\right)}{\omega_i + \omega_j}} \tag{49}$$

or, considering that δ is such that $\varepsilon\delta = 1 - \omega_k / \left(\omega_i + \omega_j\right)$,

$$\mathcal{I}_{\mathrm{t}} = \frac{\pi^2 B_{p_{ijk}}\left(\omega_i, \omega_j\right)}{2k_i k_j k_k}\frac{\omega_i\omega_j}{\frac{\omega_k - \omega_i - \omega_j}{\omega_i + \omega_j} + \mathrm{i}\frac{\omega_i\left(\xi_i + \xi_k\right) + \omega_j\left(\xi_j + \xi_k\right)}{\omega_i + \omega_j}}. \tag{50}$$

If the bispectrum of the loading is real, the imaginary part is omitted (by symmetry) and, after multiplication by 2 to account for both such peaks, the contribution of the tri-resonance peak is given by

$$m_{3,\mathrm{t}_{ijk}} = \frac{\pi^2 B_{p_{ijk}}(\omega_i,\omega_j)\,\omega_i\omega_j}{k_i k_j k_k} \frac{(\omega_k-\omega_i-\omega_j)(\omega_i+\omega_j)}{(\omega_k-\omega_i-\omega_j)^2+(\omega_i(\xi_i+\xi_k)+\omega_j(\xi_j+\xi_k))^2}. \tag{51}$$

It is important to see that this expression is equal to 0 if the equality $\omega_k = \omega_i + \omega_j$ strictly holds. Also because of the different powers of $(\omega_k - \omega_i - \omega_j)$ in the numerator and in the denominator, it decreases down to zero as $(\omega_k - \omega_i - \omega_j) \to +\infty$. In fact, this expression takes only significant values when $\omega_k - \omega_i - \omega_j$ has the same order of magnitude as the damping ratios. Indeed, in that case, the numerator is not equal to zero; it is small (same order of magnitude as the damping ratio) and the denominator is proportional to the squared damping ratio, so that $m_{3,\mathrm{t}}$ is proportional to the inverse of the damping ratio. This contribution is very similar to the resonant contribution at second order.

5.5. Summary

5.5.1. General solution

Combining (31), (41) (43), (44) and (51), the final expression obtained for the third cross-moment of the modal responses is given by

$$m_{3,ijk} = m_{3,b_{ijk}} + \left(m_{3,r_{jk}} + m_{3,r_{ik}} + m_{3,r_{ij}}\right) + m_{3,\mathrm{t}_{ijk}}. \tag{52}$$

5.5.2. Special case for equal damping and equal natural frequencies

It is possible to check that this expression boils down to the well-known solution for the singe degree-of-freedom case. Indeed, when $\omega_i = \omega_j = \omega_k$ and $\xi_i = \xi_j = \xi_k$ three contributions $m_{3,r_{jk}}$, $m_{3,r_{ij}}$ and $m_{3,r_{ik}}$ become

$$m_{3,r_{jk}} = \frac{\pi\omega_i^2}{k_i^3}\int_{\mathbb{R}} \mathrm{Re}\left[\frac{B_{p_{iii}}(\Omega,\omega_i)}{2\xi_i\omega_i - \mathrm{i}\Omega}\right]\mathrm{d}\Omega \qquad ; \qquad m_{3,r_{ik}} = \frac{\pi\omega_i^2}{k_i^3}\int_{\mathbb{R}} \mathrm{Re}\left[\frac{B_{p_{iii}}(\omega_i,\Omega)}{2\xi_i\omega_i - \mathrm{i}\Omega}\right]\mathrm{d}\Omega, \tag{53}$$

$$m_{3,r_{ij}} = \frac{\pi\omega_i^2}{k_i^3}\int_{\mathbb{R}} \mathrm{Re}\left[\frac{B_{p_{iii}}\left(-\omega_i+\frac{\Omega}{2},\omega_i+\frac{\Omega}{2}\right)}{2\xi_i\omega_i + \mathrm{i}\Omega}\right]\mathrm{d}\Omega. \tag{54}$$

Since $B_{p_{iii}}(\omega_1,\omega_2)$ is now a unilateral bispectrum, it enjoys the full symmetry properties (24) and it is possible to use these properties to show that these three results are identical, and (52) actually boils down to the solution (17) which had been previously determined for a single oscillator [24]. Furthermore, in that case, the tri-resonant contribution becomes negligible with respect to the bi-resonant contribution [24].

6. Illustrations

6.1. Exhaustive validation of the proposed formulation

The first illustration validates the simplified computation of the integrals. It is thought as a minimal working example. To do so we consider the case of a generic 3-DOF uncoupled system with natural circular frequencies

ω_i, ω_j and ω_k. Equivalently, it represents a set of any 3 modal responses in a larger structure, and only one out-of-diagonal element of the third order moment tensor, $m_{3,ijk}$, is considered.

Without any loss of generality the modal stiffnesses are considered unitary, and for the sake of simplicity all three damping ratios are assumed equal $\xi_i = \xi_j = \xi_k := \xi$. The cross-bispectrum of the loading takes the form of the square of a Gaussian process, $f(t) = \gamma \left(U + u\left(t\right)\right)^2$ so that, for small turbulence intensity σ_u/U, the bispectrum of the loading reads [41]

$$B_f\left(\omega_1, \omega_2\right) = 8\gamma^3 \left(S_u\left(\omega_1\right) S_u\left(\omega_2\right) + S_u\left(\omega_1 + \omega_2\right) S_u\left(\omega_1\right) + S_u\left(\omega_2\right) S_u\left(\omega_1 + \omega_2\right)\right). \tag{55}$$

The generating process $u(t)$ is an Ornstein-Uhlenbeck process with power spectral density

$$S_u\left(\omega\right) = \frac{1}{\pi} \frac{\alpha \sigma_u^2}{\alpha^2 + \omega^2}. \tag{56}$$

This choice makes it very simple to generate samples of $u(t)$ and $f(t)$ and compare the results of the spectral and bispectral analyses with Monte Carlo simulations.

In this illustration, the intensity of the process σ_u and the normalizing coefficient γ are chosen as $\sigma_u = 1$ and $\gamma = 1$, again without any loss of generality since they just scale the bispectrum of the loading. Furthermore, we chose $\alpha = 0.06$ as a small parameter in order to enforce the timescale separation. Indeed, the lowest natural frequency will be chosen as $\omega_i = 1$ so that only the influence of $\omega_j \left(\geq \omega_i\right)$, $\omega_k \left(\geq \omega_i\right)$ and ξ has to be studied. More precisely, the third cross-moment will be determined either (i) with an accurate numerical integration of the bispectrum, (ii) by means of the proposed formulations.

From (55) it is readily seen that the third moment of the loading is three times 8, i.e. $m_{3,f} = 24$. Because of the unit modal stiffnesses, this immediately translates into a background component (31) of the response equal to $m_{3,b} = 24$ for all considered cases. The mixed background/bi-resonant contributions (41), (43) and (44), and the tri-resonant contribution (51) admit slightly simpler expressions in the case of identical damping ratio in all three modes, see (53-54). These three components are represented on Figure 4-(a,b,c) as a function of ω_k and for $\omega_i = 1$ and various values of ω_j (1.5, 1.2, 1). They are also represented for two different damping ratios, $\xi = 0.3\%$ and $\xi = 3\%$.

The constant background $m_{3,b} = 24$ is represented by the horizontal dotted lines in the three subplots.

The mixed background/bi-resonant contributions $m_{3,r} = m_{3,r_{jk}} + m_{3,r_{ik}} + m_{3,r_{ij}}$ are represented by the solid lines. For $(\omega_i, \omega_j) = (1, 1.5)$, see Figure 4-a, the bi-resonant contribution is large when ω_k is in the neighborhood of $\omega_i = 1$ or $\omega_j = 1.5$. It is a bi-resonant contribution and is therefore more important for small damping ratio. As already discussed in [24] in the particular case of unilateral moments, the bi-resonant contribution scales with the inverse of the damping ratio only when $\xi \gtrsim \alpha$. This condition is not met here and we can observe that this component is only roughly doubled when the damping ratio is divided by 10. When ω_k is not in the neighborhood of $\omega_i = 1$ or $\omega_j = 1.5$, the bi-resonant contribution is rather small and is negligible with respect to the background. As ω_i and ω_j come closer, see Figure 4-(b,c), this component is still important when ω_k is in the neighborhood of ω_i or ω_j, but it is no longer negligible when ω_k is substantially far away from ω_i and ω_j. This simply translates the fact that this is a bi-resonant contribution and that resonance is achieved in

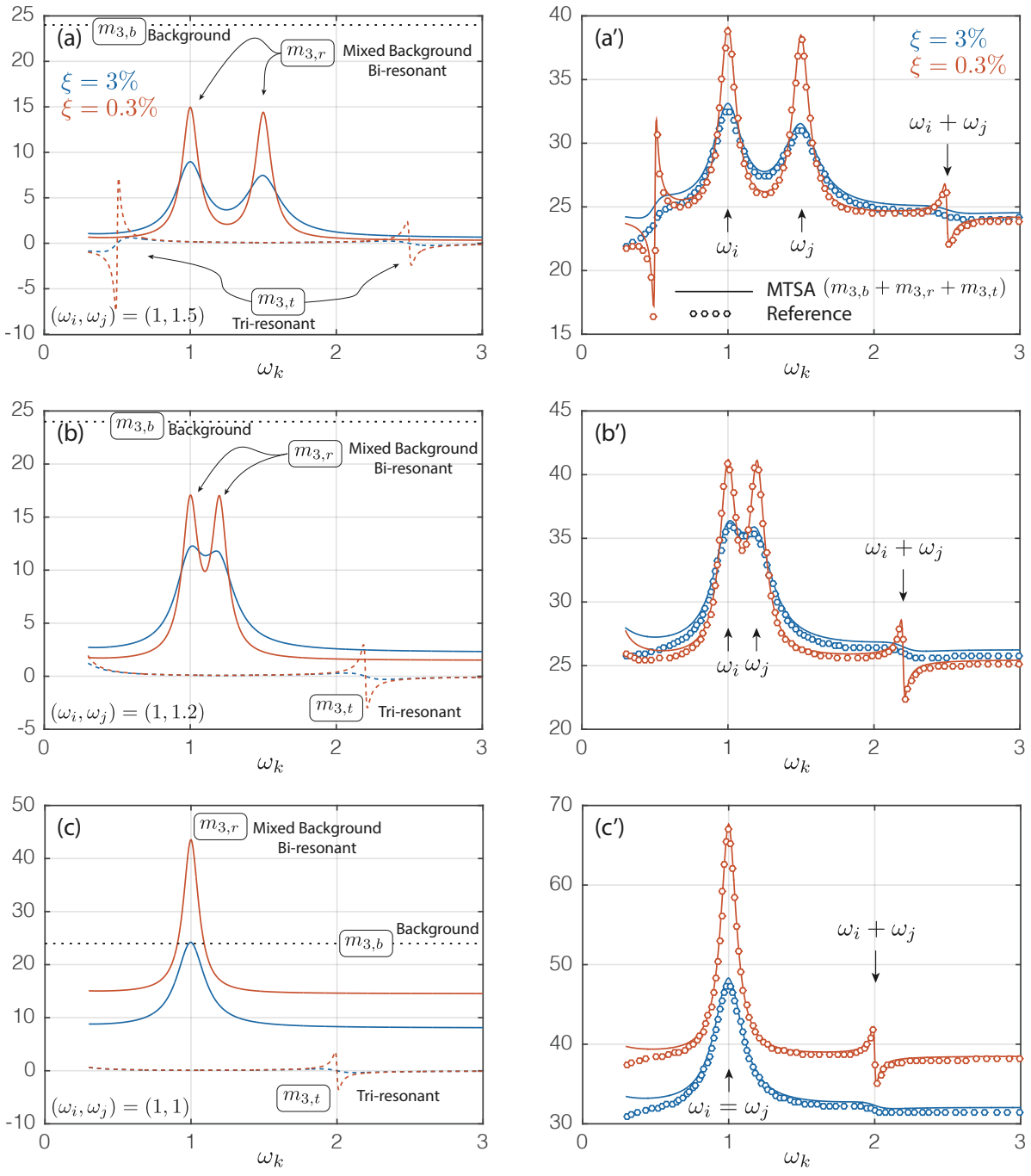

Figure 4: Cross-moment of the modal response. Left, comparison of the proposed solution (MTSA) in solid line and reference solution obtained by accurate numerical integration. Results are given for two values of the damping ratio $\xi = 0.3\%$ (red) and $\xi = 3\%$ (blue). The plot on the right provides details of the MTSA solution. Other numerical values: $\alpha = 0.06$, $\gamma = 1$, $\sigma = 1$, $\omega_i = 1$, and (a) $\omega_j = 1.5$, (b) $\omega_j = 1.2$, (c) $\omega_j = 1$.

modes i and j. Therefore, the bi-resonant contribution is important, no matter the value of ω_k. It is even more important when ω_k is also near to ω_i and ω_j. In the specific case where $\omega_i = \omega_j = \omega_k (= 1)$, see Figure 4-c, the bi-resonant contribution is as large as the background one, or even larger.

The tri-resonant contribution $m_{3,t}$ is represented by the dashed line in Figure 4-(a,b,c). This contribution is only important when the sum of two natural frequencies is close to a third one. For instance, for $(\omega_i, \omega_j) = (1, 1.5)$, see Figure 4-a, the tri-resonant contribution is large only when ω_k is in the neighborhood of $\omega_j - \omega_i = 0.5$ or $\omega_j + \omega_i = 2.5$. The plot of $m_{3,t}$ as a function of ω_k features an S-shape, crossing zero when ω_k is exactly equal to $\omega_j - \omega_i$ or $\omega_i + \omega_j$. This has been discussed together with the establishment of (51). The large slope at the crossing point translates the large sensitivity of the third statistical moment of the response to the specific values of the natural frequencies.

The sum of these three components is represented with solid lines in Figure 4-(a',b',c'). These plots, given for the same two values of the damping ratio, indicate the complex possible interactions between modal responses at third order. For comparison, the results of the proposed formulation (solid lines, MTSA) are represented together with the third statistical moments that have been obtained with an accurate numerical integration of the bispectrum. More precisely, the integral in (16) is computed with a dense and uniform mesh on the space $[-4, 4]$ with a frequency step chosen equal to $\min(\xi/2; \alpha/2)$ in order to make sure that both the background peak and the resonance peaks and crests are properly captured. The results of this numerical integration are represented with dots in Figure 4-(a',b',c'). The agreement with the proposed formulation (MTSA) is very good for all considered cases. The only major discrepancy occurs when the natural frequency ω_k is lower than about 0.5. This is because the hypothesis of timescale separation then become disputable (in this illustration $\alpha = 0.06$, so it is expected that all natural frequencies are above about 10 times α, i.e. above 0.6; below this value the timescale separation is no longer valid and the quality of the proposed decomposition worsens).

6.2. Bispectral analysis of a simple bridge model

A second example illustrates the concept of bispectral analysis and the importance of bicorrelation with a simple academic version of a 3-span bridge. The example has been designed in the manner of a benchmark in order to reveal the various features of the problem. The considered structure is represented in Figure 5. It is composed of four supports delimiting spans of 45.8m, 100m and 45.8m. The structure is therefore symmetric. It has a constant mass per unit length $\mu = 100\text{t/m}$ and bending stiffness $EI = 10^{12}\text{Nm}^2$. It is modeled with 25 finite elements on each span, which is enough to capture the first few modes very accurately. Actually, the side spans have been carefully chosen in such a way that the first three natural frequencies of this simple structure are equal to

$$\omega_1 = 4.99\text{rad/s} \quad ; \quad \omega_2 = 13.44\text{rad/s} \quad ; \quad \omega_3 = 18.32\text{rad/s},$$

so that the third natural frequency is almost equal to the sum of the first two natural frequencies. As hinted by the developments in Section 5, this will result in a possibly important tri-resonant contribution. Table 3 summarizes some important modal information: the natural frequencies, the damping ratios, the modal masses and the modal amplitudes at the position of the considered load. Rayleigh damping has been used to model structural (inherent) damping, with a target value of 1% in modes 2 and 3. It is also worth noticing that

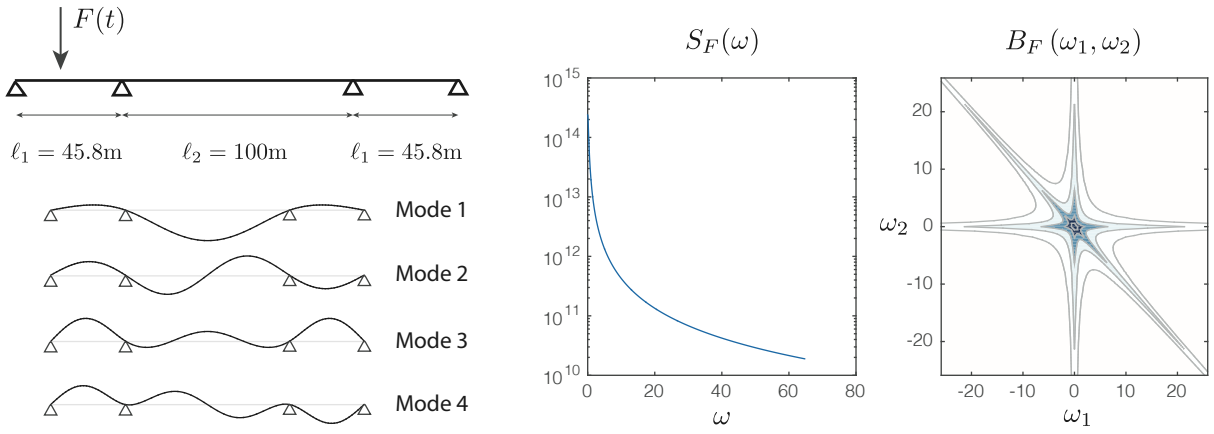

Figure 5: Sketch of the considered structure and its first four eigen modes. Power spectral density and bispectrum of the unique considered load.

Mode	ω_i [rad/s]	ξ_i	M_i [to]	$\phi_{F,i}$
1	4.99	1.71%	4717	0.132
2	13.4	1.00%	7434	0.601
3	18.3	1.00%	5009	0.884
4	21.6	1.04%	6294	0.918

Table 3: Summary of important modal properties

only one degree-of-freedom of the model will be considered to be loaded. The modal displacements $\phi_{F,i}$ at this degree-of-freedom grow from 0.132 to 0.918 with the number of the mode. All these particular choices have been made to design a simple example where the structure significantly responds in four modes and in such a way that modal correlation is not negligible. It is clear that this example does not represent a particular application but is constructed as the simplest possible example that is suitable to illustrate the concept of bicorrelation.

The only loaded degree-of-freedom is the transverse displacement at node 9, i.e. located at a distance of 15.52m from the left end of the beam. The force assumes a quadratic transformation of a Gaussian process, as it would be in a buffeting analysis,

$$F(t) = \gamma \left(1 + \frac{w\,(t)}{U}\right)^2 \tag{57}$$

where $\gamma = \frac{1}{2}\rho B U^2 c_A = 45 \cdot 10^3$kN and where the turbulence $w(t)$ is supposed to be a Gaussian process with PSD given by the von Karman spectrum [4],

$$S_w\,(\omega) = \frac{4L_w\sigma_w^2}{U} \frac{1 + 755.2\,(nL_w/U)^2}{\left[1 + 283.2\,(nL_w/U)^2\right]^{11/6}} \tag{58}$$

where $U = 30$ m/s is the average wind speed, $L_w = 100$ m is the integral length scale and $\sigma_w = 5$ m/s is the standard deviation of the fluctuation in the wind speed.

This information is sufficient to construct a finite element model of the structure and compute the displacements and bending moments along the structure. For convenience, the mass $\mathbf{M}$, stiffness $\mathbf{K}$ and damping

C matrices are available for download, as well as the Matlab code used to compute the structural responses and construct the graphs shown in the sequel (Note for reviewers: this material will be available after paper acceptance). The size of the structural matrices is 148×148 and the displacements and bending moments are computed at the 76 nodes of the model.

The structural response is computed in two different ways. First, a Monte Carlo approach is considered, where samples of the turbulence $w(t)$ are generated and samples of the force $F(t)$ are constructed with (57). A time step $\Delta t = 0.01$ s is used. It is necessary to use such a short time step in order to accurately capture the dynamics in mode 4, which has natural period $T_4 = 2\pi/\omega_4 = 0.29$ s, i.e. $\Delta t/T_4 \simeq 1/30$. Also, the total duration of the simulation is covered by $2 \cdot 10^6$ time steps, i.e.a duration of 20000 seconds. This long simulation duration is necessary to obtain reasonably well converged statistics, as shown next. Indeed, once the samples of structural displacements and bending moments are obtained, statistics such as standard deviation, PSD and skewness coefficients can be determined. They need to be reproducible from one run to another, i.e. limit their dependence to sampling, which justifies this long simulation time. This first way of performing the structural analysis develops into two different ways, either in the nodal basis, either in the modal basis. In this latter case, the normal modes of vibrations shown in Figure 5 are used.

The second investigation option relies on the spectral and bispectral analyses. For small turbulence intensity, it is possible to show that the power spectral density and the bispectrum of the force applied in the left span are given by

$$S_F(\omega) = 4\gamma^2 S_w(\omega) \quad ; \quad B_F(\omega_1, \omega_2) = 8\gamma^3 \left[S_w(\omega_1 + \omega_2) S_w(\omega_1) + S_w(\omega_1) S_w(\omega_2) + S_w(\omega_1 + \omega_2) S_w(\omega_2) \right] \tag{59}$$

They are represented in Figure 5. These expressions assume that the turbulence intensity is small. The complete expression is given in Appendix A. Later comparison with the Monte Carlo approach in the time domain will confirm that these simpler leading order expressions can be used. The flow of the spectral analysis has been recalled in Section 3. It consists in the computation of the spectra and bispectra of modal forces, modal responses, followed by the variances, covariances and third (cross-)moments of modal responses. Ultimately, these modal responses are recombined with the CQC/SRSS and CCC/CRSC methods in order to obtain the statistics of nodal displacements and bending moments.

Figure 6-a show samples of the modal responses in the first four modes, which are the only ones retained for the analysis. A closeup view is also given in Figure 6-a', which better illustrates that the modal responses are well composed of a slowly varying background response and fast oscillations. This is also confirmed by the PSDs represented in Figure 6-b. The slightly erratic lines correspond to the Monte Carlo simulation in the time domain. They fit almost perfectly the PSDs obtained in the spectral analysis, see the dashed lines. This only discrepancy between the two results lies in the higher frequency ranges, where the time domain analysis is seen to slightly overestimate the actual frequency content. This is due to a well-known limited filtering capability of the Newmark algorithm taking place when the time step is (relatively) large. Since this difference occurs at very low levels; it does not alter the estimation of the variance. Indeed, the second order moments (variances and covariances) are represented in Figure 6-c, which indicates very little difference between the time domain

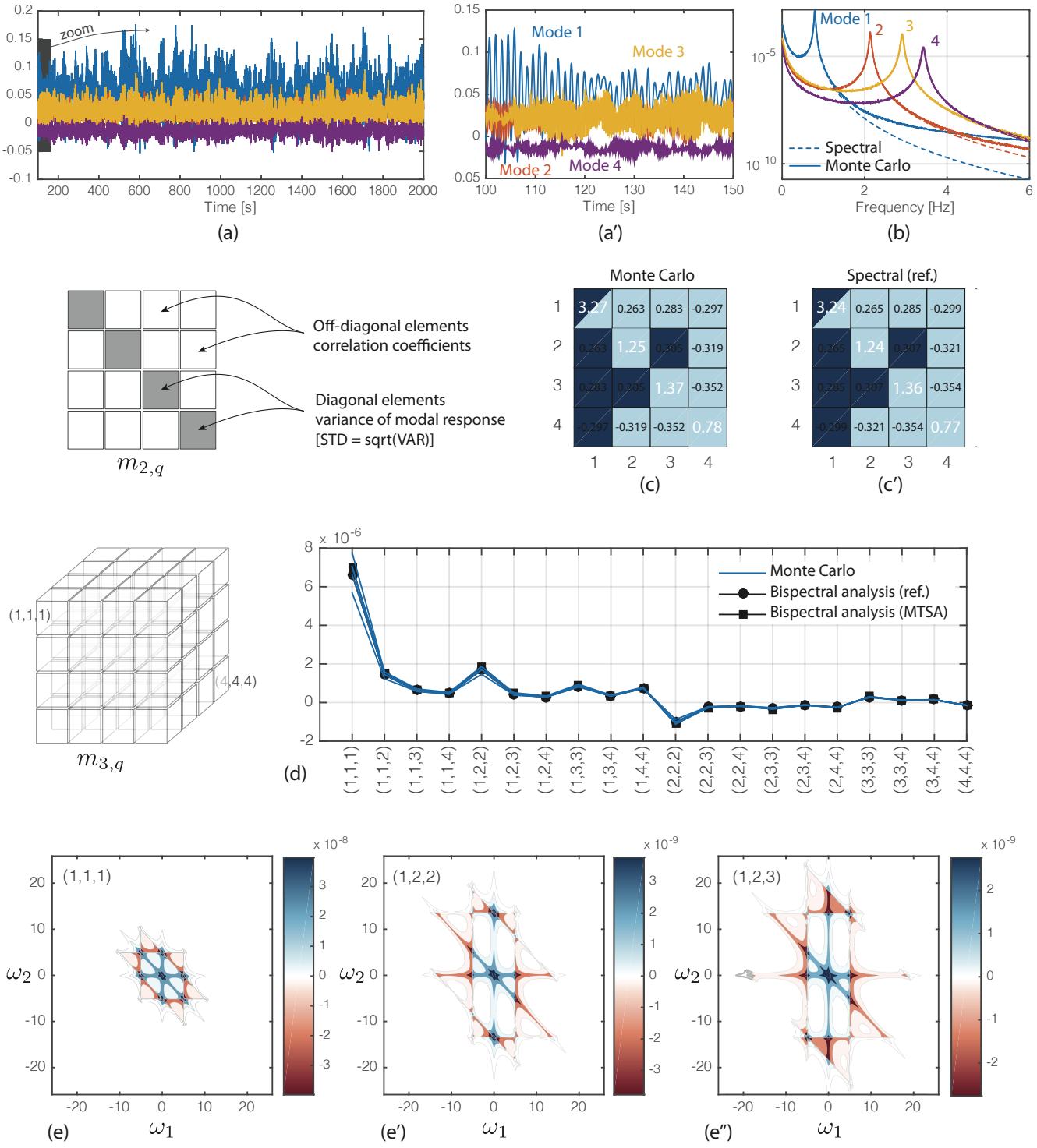

Figure 6: Illustration of modal responses. (a) Time series of modal responses, (b) comparison of the PSDs of modal responses obtained in the time domain (Monte Carlo simulations) and in the spectral approach at second order, (c) covariance matrices of modal responses (numerical values given on the diagonal are the standard deviations of modal responses in cm, out-of-diagonal values represent correlation coefficients), (d) bicovariance matrices of modal responses, represented element by element (comparison of three methods of analysis), (e) selected bispectra and cross-bispectra of modal responses (real part).

and the spectral approaches. The values given in the diagonal elements of these matrices represent the standard deviations of the modal responses (in centimeters) while the off-diagonal elements represent the correlation coefficients. The two approaches agree very well. It is also observed that the correlation coefficients are all located around the same value (~ 0.3). This is due to the fact that all modes respond with about 30% in the background regime and that there is only one nodal load applied on this structure.

Figure 6-d shows the elements of the third statistical moments of modal responses, $m_{q,ijk}$. Because of symmetry only 20 elements out of the 64 elements of $\mathbf{m}_{3,q}$ are different. The largest one is (1,1,1), which corresponds to the unilateral moment in the first mode. Then (1,2,2) and (2,2,2) are quite significant in absolute value. The plot indicates that the third statistical moments involving mode 4 are smaller, i.e. there is a smaller tendency to non Gaussianity in higher modes. This graphs also compares three approaches. The first two are: the time domain simulation with a large number of time steps ($N = 2 \cdot 10^6$) and the bispectral analysis with a large number of integration points (179284 points are located in the half-plane $(\omega_1, \omega_2) \in [0, 64.7] \times [-64.7; 64.7]$ (rad/s) at selected positions in order to provide accurate integrals). These two results match very well. We highlight that the five repeated runs of the Monte Carlo simulation, represented by the five solid lines, do not exactly yield the same results. This indicates that the large number of time steps ($N = 2 \cdot 10^6$) should have been chosen even larger to provide statistically converged results. The third result represented in Figure 6-d is obtained with the proposed method (MTSA), that is the decomposition of the third cross-moments with the sum of three components as given in (52).

Last but not least, Figure 6-e illustrates a selection of bispectra of modal responses. They exhibit the same features as those shown in Figure 3. In particular, the symmetric nature of the unilateral bispectrum is remarkable while this symmetry is broken for cross-bispectra. The values of the cross-moments shown in 6-d are the integrals of such spectra.

Figure 7 shows the standard deviation and the skewness coefficient of the displacement and bending moment all along the structure. Again, the results of the time domain simulation are represented by solid lines. In each graph, the results of 5 Monte Carlo simulations are represented. For the standard deviations, the results are virtually superimposed so that it is difficult to distinguish them; however, for the skewness coefficient a slight scatter is visible, which confirms again that long simulations are necessary to reach accurate third order moments. The gray solid lines correspond to time domain simulations in the nodal basis, i.e. without modal truncation. The blue solid lines correspond to analysis in the modal basis and the complete (quadratic or cubic) combination. These two sets of results seem to match, which validates the use of the modal basis for the analysis of this structure. The major discrepancy is the bending moment under the applied load, which is expected since the mode shapes are not able to capture the discontinuity in the shear force. To a lesser extent, the skewness coefficient of the bending moment is slightly affected by the truncation, although the global profile is acceptable. The red solid lines correspond to time domain analysis in the modal basis, but recombination is made with the diagonal elements only of the covariance matrix $m_{2,q}$ (SRSS combination) and of the third moment matrix $m_{3,q}$ (CRSC combination). The difference between these two sets of displacement and bending moment profiles highlights the importance of correlations. While at second order, this phenomenon is already well understood,

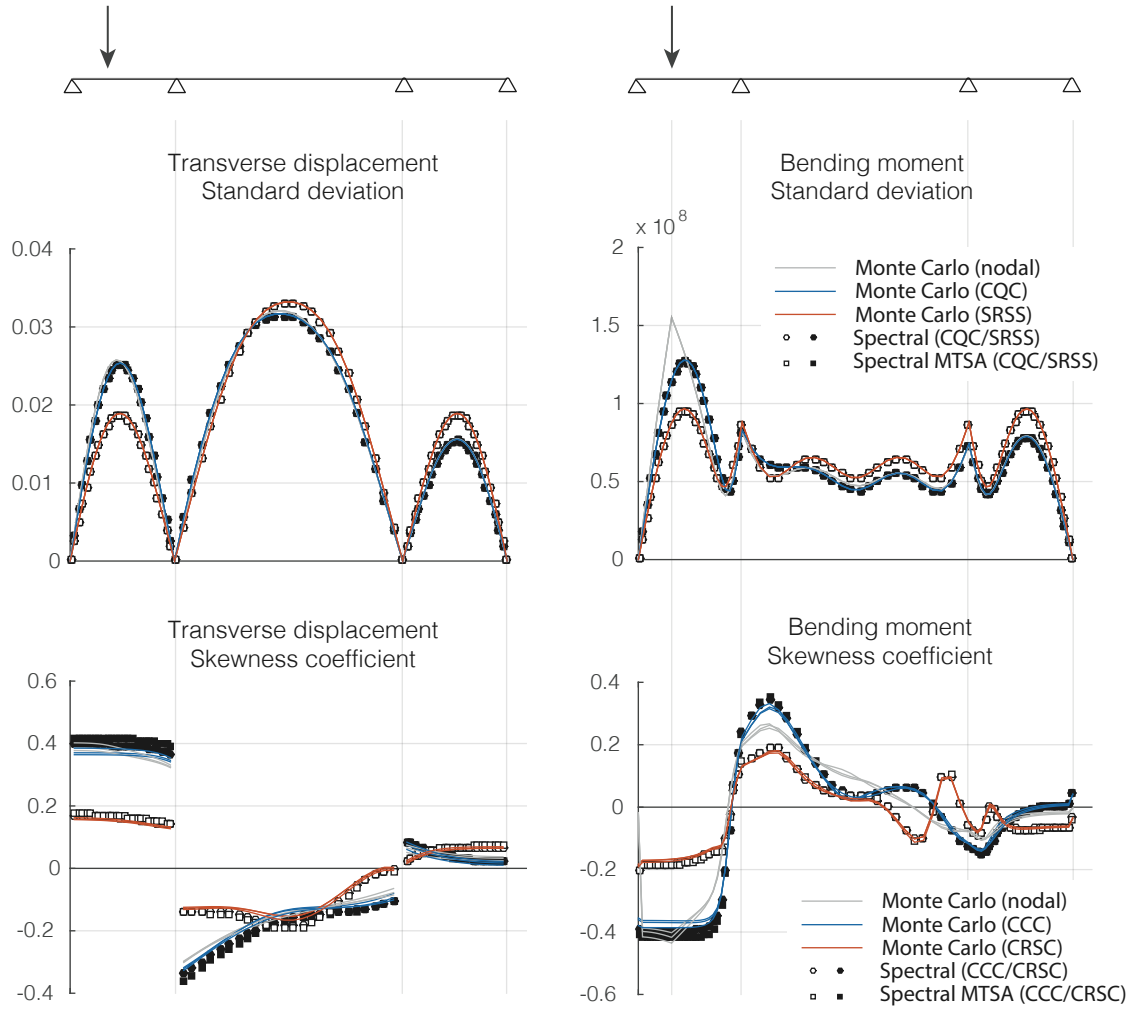

Figure 7: Standard deviation and skewness coefficient of the transverse displacement and bending moments along the beam.

Analysis method	Runtime [s]	Normalized runtime [-]
Time domain, Nodal basis	126.5 (per run)	× 183
Time domain, Modal basis	138.9 (per run)	× 201
Spectral & bispectral	48.7	× 70
MTSA (proposed method)	0.69	× 1

Table 4: Comparison of the different analysis method with respect to computational time.

this illustration is the first occasion to show distributions of skewness coefficients along a structure highlighting the difference between these two recombinations techniques. Differences as large as a factor of 2 are obtained for the skewness of the bending moment and of the transverse displacement in the first span.

More importantly, this paper aims at showing that it is possible to recover the same results with a bispectral analysis. The black dots and squares indicate, in Figure 7, the structural responses (displacement and bending moments) obtained in a frequency domain. They match almost perfectly the time domain simulation. Also, the results obtained with the reference spectral and bispectral analysis (dots) are virtually the same as those obtained with the proposed decomposition (MTSA), which are represented by small squares. This is naturally expected since the agreement was already very good for modal responses.

Finally, Table 4 shows the massive saving in computational time for the structural analysis. The Monte Carlo simulation takes about 2 minutes to complete, per run. In the previous analysis, we have repeated each analysis 5 times in order to make sure the simulation time was long enough. In principle, the total computational cost should have been multiplied by this number of repetitions. Furthermore, the small residual dispersions observed in the skewness coefficients show that it is not reasonable to decrease the number of time steps. So about 2 minutes can be considered as a best score for the Monte Carlo approach. Nodal or modal basis does not change much. For such a small model the saving in the reduction of the size of the basis is compensated by the time required for the modal projection. The spectral and bispectral analysis is 2 to 3 times faster. This is for the same accuracy, since results of the structural analysis match very well. The proposed method, on top of providing results of similar quality, completes the same task yet 70 times faster than the complete and accurate integration. This results from the fact that the third moment is now obtained with a single integral instead of a twofold integral. The second column in Table 4 provides the normalized runtime, with respect to the fastest method.

6.3. Perspectives on the estimation of peak factors

Before closing, it is interesting to return to the original question of any non Gaussian analysis: extreme values. They are of utmost importance to designers, since they are the final results for design. In a time domain analysis, they are determined as the average maximum (respectively minimum) values observed over a certain window T, chosen as $T = 600$s in this illustration. In a spectral analysis, the extreme values, minimum and maximum, of any response quantity z are determined by

$$z_{\max} = \bar{z} + g_{\mathrm{MAX}}\sigma_z \qquad z_{\min} = \bar{z} - g_{\mathrm{MIN}}\sigma_z \tag{60}$$

γ_3	-0.4	-0.3	-0.2	-0.1	0	0.1	0.2	0.3	0.4
g_{MAX}	3.06	3.28	3.50	3.73	3.98	4.23	4.48	4.75	5.02
g_{MIN}	5.02	4.75	4.48	4.23	3.98	3.73	3.50	3.28	3.06

Table 5: Peak factors expressed as a function of the skewness coefficient (Kareem-Zhao model).

where $\bar{z}$ and σ_z represent the average value and standard deviation of the response z (e.g. displacement, bending moment), and g_{MAX} and g_{MIN} are the peak factors. For Gaussian processes, the peak factor is usually determined by means of the so-called Rice's formula, $g = \beta + 0.5772/\beta$ (with $\beta = \sqrt{2\ln \nu_0 T}$), assuming Poissonian crossings of maximum values [42, 43, 44]. Assuming a zero upcrossing rate $\nu_0 = 2.5$Hz as an average value of the natural frequencies in the first four modes, this formula gives $g_{\mathrm{MAX}} = g_{\mathrm{MIN}} = 3.98$. For non Gaussian (skewed) processes, the probability distribution function of the response is no longer symmetric, $g_{\mathrm{MAX}} \neq g_{\mathrm{MIN}}$, and more advanced peak factor models need to be used. Among them, the model proposed by Zhao and Kareem [45], based on a cubic translation, looks simple enough, although suspected to slightly overestimate the actual peak factors [44]. It actually requires estimation of the excess coefficient γ_e, which is unfortunately unknown here since the analysis stopped at third order. Since this part of the discussion is just to open perspectives, it is decided to keep using this model and simply assume that the couple (γ_3, γ_e) composed of the skewness and excess coefficients lies on the limit of the so-called monotone region [46, 47, 48, 49]. Examples of applications in wind engineering indicate that this assumption is close to reality. With this, the peak factors g_{MAX} and g_{MIN} are explicitly obtained from γ_3, once ν_0 and T are fixed. Some numerical values of the peak factors obtained with this approach are summarized in Table 5.

Figure 8-a shows the extreme values obtained for the five Monte Carlo simulations in solid lines. The repeatability of the analysis is very good. Also it matches very well the estimates obtained with the proposed bispectral approach (MTSA). This latter one is based on (60) where: the average value $\bar{z}$ is obtained from a static analysis, the standard deviation is obtained with a classical spectral analysis, and the skewness coefficient γ_3 of the displacements and bending moments is computed as in (20), where the third moment is obtained with the proposed MTSA approach. Then the peak factor is obtained with the Kareem-Zhao model, for which some numerical values are given in Table 5 (to be interpolated).

The matching is in fact remarkable, especially knowing that the proposed method is about 200 times faster. The remaining plots in Figure 8 show detailed information about this extreme value analysis. In particular, Figure 8-b shows the peak factors along the bridge, either computed with the Kareem-Zhao approach, either obtained with the Monte Carlo analysis, i.e. $(\max - \text{average})/\text{std}$ or $(\text{average} - \min)/\text{std}$. The agreement is appreciable which hints that the skewness coefficient alone can be used as a good proxy to get the peak factor. The discrepancy in the first span can be related to modal truncation issues, as already revealed by Figure 7. Finally, Figures 8-(c,d) give the cross plots of the skewness coefficients and the peak factors of bending moments at each node of the model. The results obtained with the Monte Carlo simulation indicate again that the model of Zhao and Kareem (values can be found in Table 5) is accurate enough despite the simplifying assumptions.

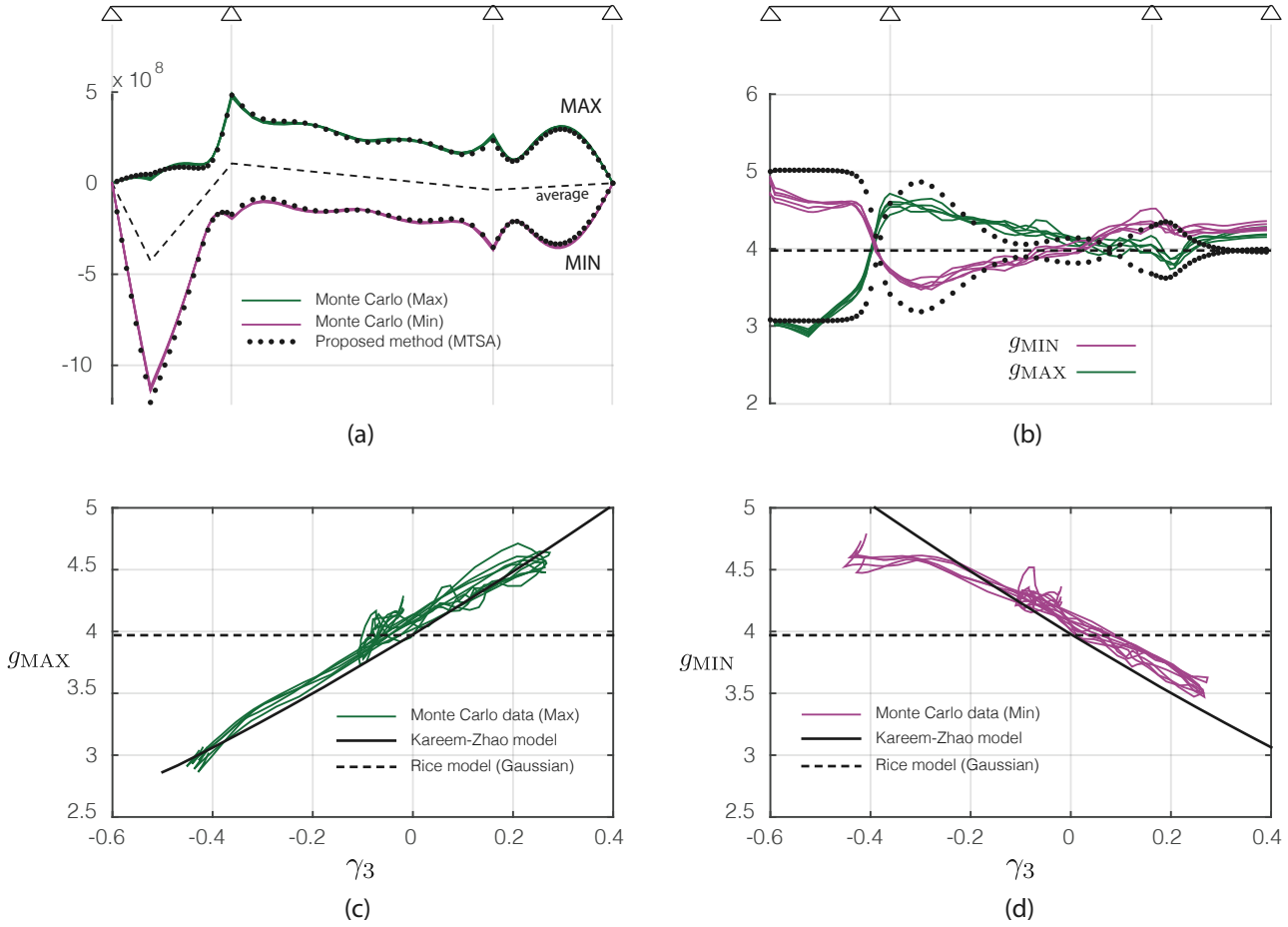

Figure 8: (a) Extreme values (max and min) obtained with the Monte Carlo simulations and with the proposed bispectral approach, (b) comparison of the peak factors, (c-d) representation of peak factors as a function of the skewness coefficient (Monte Carlo: obtained from simulated data; Kareem-Zhao model: used in the bispectral analysis).

7. Conclusions

In this paper, we have identified the different components of the third order cross-moments of modal responses of structures subjected to low-frequency loading. For each of them we have derived the simplest possible expressions, owing to the small structural damping (less than about 10%) and the timescale separation. These expressions are particularly useful and offer new perspectives as to the accurate analysis of large structures subjected to non Gaussian wind loads.

Among the three main contributions to the cross-moments, the background and the bi-resonant components are very similar to the contributions exisiting for unilateral moments. Beside, we have shown the existence of another component, namely the tri-resonant component, which makes a significant difference compared to the unilateral case. It can become virtually very large compared to unilateral moment (especially when damping is low). This only appears when one natural frequency is close to the sum of two others. This condition is rather rare in small structures but could easily be met in large multi-span structures.

Before the existence of the proposed decomposition of the response into these three components, the analysis of large systems subject to complex wind fields was only viable in the time domain. And yet, the illustration of the previous Section has indicated that very long simulation times are required to obtain accurate results and according to our analysis of the literature, we could not identify existing examples of sufficiently long simulations (that could accurately return third or higher statistical moments) for large structures.

The computational burden associated with the spectral and bispectral analyses with accurate numerical integration would significantly grow for more complex structures. It was affordable for the illustration given in the previous section, but would quickly become difficult to implement for larger structures. Moreover, in the second example, we could drastically simplify the analysis because there was only one loaded point. Transposition of the same analysis to a structure with more loaded points would scale up the computational burden in proportion to the cube of the number of loads, but also of the number of modes. This explains why the formal bispectral analysis is usually not conducted for large structures.

However, with the help of the proposed decomposition, we see that the computational burden associated with the computation of each moment becomes so small that it is not feared any longer to repeat this operation a large number of times. For these reasons, the proposed method appears as a very interesting way, perhaps the only one today, to perform the non Gaussian dynamic analysis of large structures, within a reasonable computational time. The proposed formulation has eventually been compared to a Monte Carlo simulation approach and has shown a computation speedup expressed by a factor of about 200. Future simulations and applications to larger structures should confirm that this efficiency is also valid in more realistic applications, as discussed hereabove.

8. Acknowledgements

This paper was partly supported by a doctoral grant of the FNRS (Belgian Fund for Scientific Research) attributed to Margaux Geuzaine. Her work was also funded by two research stay grants from the FWB (Fédération Wallonie-Bruxelles) and the Rotary. As for the involvement of Michele Esposito Marzino in this project,

it was made possible thanks to the research project FINELG2020, which is supported by the Service Public de Wallonie.

Appendix A

Let $w(t)$ be a zero-mean Gaussian random process with given power spectral density (PSD) $S_w(\omega)$ and variance σ_w^2. It is possible to prove [41, 25] that the PSD and bispectrum of a squared transformation of $w(t)$, such as $F(t) = \gamma\left(1 + w(t)/U\right)^2$ are given by the following expressions. The PSD reads

$$S_F(\omega) = \frac{4\gamma^2}{U^2} S_w(\omega) + \frac{2\gamma^2}{\bar{U}^4} \int_{-\infty}^{+\infty} S_w(\omega_1) S_w(\omega - \omega_1)\, d\omega_1. \tag{61}$$

Integration of this quantity of the frequency space yields

$$\sigma_F^2 = \gamma^2 \left(4\frac{\sigma_w^2}{U^2} + 2\frac{\sigma_w^4}{\bar{U}^4}\right) = 4\gamma^2 I_w^2 \left(1 + \frac{I_w^2}{2}\right) \tag{62}$$

where the turbulence intensity I_w usually assumes small values in Wind Engineering (10%-30%). Therefore, the second term is much smaller than the first one and the second terms in (61) can be neglected. This is the approach followed here. Comparison with the Monte Carlo simulation results in the second illustration indicate that this assumption is acceptable.

This complete expression of the bispectrum of the force is given by

$$\begin{aligned} B_F(\omega_1, \omega_2) = {} & \frac{8\gamma^3}{U^4} \left[S_w(\omega_1 + \omega_2) S_w(\omega_1) + S_w(\omega_1) S_w(\omega_2) + S_w(\omega_1 + \omega_2) S_w(\omega_2)\right] \\ & + \frac{8\gamma^3}{U^6} \int_{-\infty}^{+\infty} S_w(\omega + \omega_1) S_w(\omega) S_w(\omega_2 - \omega)\, d\omega. \end{aligned} \tag{63}$$

The third statistical moment associated with this bispectrum, obtained by a double integration along frequencies in (ω_1, ω_2) is equal to

$$m_{3,F} = 8\gamma^3 \left[3\frac{\sigma_w^4}{U^4} + \frac{\sigma_w^6}{U^6}\right] = 24\gamma^3 I_w^4 \left(1 + \frac{I_w^2}{3}\right). \tag{64}$$

Again, because of the small turbulence intensity, the second term can be omitted, which explains the form considered in (59). For the record, the skewness coefficient of the loading, expressed by (20), is equal to $\gamma_{3,F} = m_{3,F}/\sigma_F^3 = 3I_w$. In the considered application $I_w = 5/30 = 0.167$, so that the skewness of the loading is $\gamma_{3,F} = 0.5$.

References

[1] André Preumont. Random vibration and spectral analysis. 1994.

[2] Loren D Lutes and Shahram Sarkani. *Random vibrations: analysis of structural and mechanical systems.* Butterworth-Heinemann, 2004.

[3] Jie Li and Jianbing Chen. *Stochastic dynamics of structures*. John Wiley & Sons, 2009.

[4] Ahsan Kareem and Yukio Tamura. *Advanced structural wind engineering*, volume 482. Springer, 2013.

[5] John D Holmes. *Wind loading of structures*. CRC press, 2007.

[6] MP Paıdoussis and GX Li. Pipes conveying fluid: a model dynamical problem. *Journal of fluids and Structures*, 7(2):137–204, 1993.

[7] Hugo Bachmann and Walter Ammann. *Vibrations in structures: induced by man and machines*, volume 3. Iabse, 1987.

[8] Giuseppe Piccardo and Federica Tubino. Equivalent spectral model and maximum dynamic response for the serviceability analysis of footbridges. *Engineering Structures*, 40:445–456, 2012.

[9] Michel Géradin and Daniel J Rixen. *Mechanical vibrations: theory and application to structural dynamics*. John Wiley & Sons, 2014.

[10] Vincent Denoël and Hervé Degée. Asymptotic expansion of slightly coupled modal dynamic transfer functions. *Journal of Sound and Vibration*, 328(1-2):1–8, 2009.

[11] G Borino and G Muscolino. Mode-superposition methods in dynamic analysis of classically and non-classically damped linear systems. *Earthquake engineering & structural dynamics*, 14(5):705–717, 1986.

[12] Vincent Denoël. Estimation of modal correlation coefficients from background and resonant responses. *Structural Engineering and Mechanics: an International Journal*, 32(6), 2009.

[13] Edward L Wilson, Armen Der Kiureghian, and EP Bayo. A replacement for the srss method in seismic analysis. *Earthquake Engineering & Structural Dynamics*, 9(2):187–192, 1981.

[14] WB Collis, PR White, and JK Hammond. Higher-order spectra: the bispectrum and trispectrum. *Mechanical systems and signal processing*, 12(3):375–394, 1998.

[15] Sang-Won Nam and Edward J Powers. Application of higher order spectral analysis to cubically nonlinear system identification. *IEEE Transactions on Signal Processing*, 42(7):1746–1765, 1994.

[16] IM Howard. Higher-order spectral techniques for machine vibration condition monitoring. *Proceedings of the Institution of Mechanical Engineers, Part G: Journal of Aerospace Engineering*, 211(4):211–219, 1997.

[17] Vittorio Gusella and Annibale Luigi Materazzi. Non-gaussian response of mdof wind-exposed structures: analysis by bicorrelation function and bispectrum. *Meccanica*, 33(3):299–307, 1998.

[18] Wenliang Fan, Xiangqian Sheng, Zhengliang Li, and Yi Sun. The higher-order analysis method of statistics analysis for response of linear structure under stationary non-gaussian excitation. *Mechanical Systems and Signal Processing*, 166:108430, 2022.

[19] Zhiwei Xu, Gonglian Dai, Limao Zhang, Y Frank Chen, Richard GJ Flay, and Huiming Rao. Effect of non-gaussian turbulence on extreme buffeting response of a high-speed railway sea-crossing bridge. *Journal of Wind Engineering and Industrial Aerodynamics*, 224:104981, 2022.

[20] Nicolas Blaise, Thomas Canor, and Vincent Denoël. Reconstruction of the envelope of non-gaussian structural responses with principal static wind loads. *Journal of Wind Engineering and Industrial Aerodynamics*, 149:59–76, 2016.

[21] Ahsan Kareem and Teng Wu. Wind-induced effects on bluff bodies in turbulent flows: Nonstationary, non-gaussian and nonlinear features. *Journal of Wind Engineering and Industrial Aerodynamics*, 122:21–37, 2013.

[22] Shunji Kato and S Ando. Statistical analysis of low frequency responses of a moored floating offshore structure.(1st report). (23):17–58, 1986.

[23] Margaux Geuzaine and Vincent Denoël. Efficient estimation of the skewness of the response of a wave-excited oscillator. In *EURODYN 2020: XI International Conference on Structural Dynamics*, 2020.

[24] Vincent Denoël. On the background and biresonant components of the random response of single degree-of-freedom systems under non-gaussian random loading. *Engineering structures*, 33(8):2271–2283, 2011.

[25] Vincent Denoël and Luigi Carassale. Response of an oscillator to a random quadratic velocity-feedback loading. *Journal of Wind Engineering and Industrial Aerodynamics*, 147:330–344, 2015.

[26] Ananthram Swami, Jerry M Mendel, and Chrysostomos L Nikias. Higher-order spectral analysis toolbox. *The Mathworks Inc*, 3:22–26, 1998.

[27] Alan Garnett Davenport. The application of statistical concepts to the wind loading of structures. *Proceedings of the Institution of Civil Engineers*, 19(4):449–472, 1961.

[28] Rouslan L Stratonovich. *Topics in the theory of random noise*, volume 2. CRC Press, 1967.

[29] Vincent Denoël. Extension of the background/biresonant decomposition to the estimation of the kurtosis coefficient of the response. In *Uncertainty in Structural Dynamics*, 2012.

[30] Vincent Denoël. Extension of davenport's background/resonant decomposition for the estimation of higher response moments. In *6th European-African Conference on Wind Engineering*, 2013.

[31] Vincent Denoël. Multiple timescale spectral analysis. *Probabilistic Engineering Mechanics*, 39:69–86, 2015.

[32] Thomas Canor, Nicolas Blaise, and Vincent Denoël. Efficient uncoupled stochastic analysis with non-proportional damping. *Journal of Sound and Vibration*, 331(24):5283–5291, 2012.

[33] Andreas Kappos. *Dynamic loading and design of structures*. CRC Press, 2001.

[34] Ahsan Kareem, Jun Zhao, and Michael A Tognarelli. Surge response statistics of tension leg platforms under wind and wave loads: a statistical quadratization approach. *Probabilistic Engineering Mechanics*, 10(4):225–240, 1995.

[35] J. D. Holmes. Non-Gaussian Characteristics Of Wind Pressure Fluctuations. *Journal of Wind Engineering and Industrial Aerodynamics*, 7:103–108, 1981.

[36] Anil K Chopra. Modal combination rules in response spectrum analysis: Early history. *Earthquake Engineering & Structural Dynamics*, 50(2):260–269, 2021.

[37] Armen Der Kiureghian. Structural response to stationary excitation. *Journal of the Engineering Mechanics Division*, 106(6):1195–1213, 1980.

[38] Hans Wolfgang Liepmann. On the application of statistical concepts to the buffeting problem. *Journal of the Aeronautical Sciences*, 19(12):793–800, 1952.

[39] Margaux Geuzaine, Michele Esposito Marzino, and Vincent Denoël. Efficient estimation of the skewness of the response of a linear oscillator under non-gaussian loading. Engineering Mechanics Institute conference, 2020.

[40] Jirayr Kevorkian and Julian D Cole. *Perturbation methods in applied mathematics*, volume 34. Springer Science & Business Media, 2013.

[41] Vincent Denoël and Hervé Degée. Influence of the non-linearity of the aerodynamic coefficients on the skewness of the buffeting drag force. *Wind and Structures*, 9(6), 2006.

[42] Stephen O Rice. Mathematical analysis of random noise. *The Bell System Technical Journal*, 23(3):282–332, 1944.

[43] Alan Garnett Davenport. Note on the distribution of the largest value of a random function with application to gust loading. *Proceedings of the Institution of Civil Engineers*, 28(2):187–196, 1964.

[44] T Ishikawa. A study on wind load estimation method considering dynamic effect for overhead transmission lines. *Doctoral thesis, Waseda University*, 2004.

[45] A. Kareem and J. Zhao. Analysis of non-gaussian surge response of tension leg platforms under wind loads. *Journal of Offshore Mechanics and Arctic Engineering*, 116(3):137–144, 1994.

[46] Myoungkeun Choi and Bert Sweetman. The hermite moment model for highly skewed response with application to tension leg platforms. *Journal of offshore mechanics and Arctic engineering*, 132(2), 2010.

[47] Xinlai Peng, Luping Yang, Eri Gavanski, Kurtis Gurley, and David Prevatt. A comparison of methods to estimate peak wind loads on buildings. *Journal of wind engineering and industrial aerodynamics*, 126:11–23, 2014.

[48] Luping Yang, Kurtis R. Gurley, and David O. Prevatt. Probabilistic modeling of wind pressure on low-rise buildings. *Journal of Wind Engineering and Industrial Aerodynamics*, 114:18–26, 2013.

[49] Qingshan Yang and Yuji Tian. A model of probability density function of non-gaussian wind pressure with multiple samples. *Journal of Wind Engineering and Industrial Aerodynamics*, 140:67–78, 2015.